Neurobiology of Stress 15 (2021) 100402

Contents lists available at ScienceDirect

Neurobiology of Stress

journal homepage: www.elsevier.com/locate/ynstr

Dual imaging of dendritic spines and mitochondria *in vivo* reveals hotspots of plasticity and metabolic adaptation to stress

Yann Dromard [a], Margarita Arango-Lievano [a], Pierre Fontanaud [a,b], Nicolas Tricaud [c], Freddy Jeanneteau [a,*]

[a] Institut de Génomique Fonctionnelle, Université de Montpellier, INSERM, CNRS, 34090, Montpellier, France
[b] Imagerie du petit animal de Montpellier, 34090, Montpellier, France
[c] I-Stem, UEVE, INSERM, AFM, 91100, Corbeil-Essonnes, France

ARTICLE INFO

Keywords:
Chronic unpredictable stress
Dendritic spine
Mitochondria
Clustering
In vivo microscopy

ABSTRACT

Metabolic adaptation is a critical feature of synaptic plasticity. Indeed, synaptic plasticity requires the utilization and resupply of metabolites, in particular when the turnover is high and fast such as in stress conditions. What accounts for the localized energy burden of the post-synaptic compartment to the build up of chronic stress is currently not understood. We used *in vivo* microscopy of genetically encoded fluorescent probes to track changes of mitochondria, dendritic spines, ATP and H2O2 levels in pyramidal neurons of cortex before and after chronic unpredictable mild stress. Data revealed hotspots of postsynaptic mitochondria and dendritic spine turnover. Pharmacogenetic approach to force expression of the metabolic stress gene *NR4A1* caused the fragmentation of postsynaptic mitochondria and loss of proximal dendritic spine clusters, whereas a dominant-negative mutant counteracted the effect of chronic stress. When fragmented, dendritic mitochondria produced lesser ATP at resting state and more on acute demand. This corresponded with significant production of mitochondrial H2O2 oxidative species in the dendritic compartment. Together, data indicate that pyramidal neurons adjust proximal dendritic spine turnover and mitochondria functions in keeping with synaptic demands.

1. Introduction

Exhaustion of energy in the brain is unlikely because mitochondrial and glycolytic metabolisms continuously provide the ATP that sustains neuronal activity (Ashrafi et al., 2017; Devine and Kittler, 2018; Harris et al., 2012; Jang et al., 2016). Besides energy, mitochondria also provide oxidative radicals and Ca^{2+} homeostasis required for synaptic functions (Fu et al., 2017; Kwon et al., 2016; Vaccaro et al., 2017). In the pre-synapse, mitochondria are a major source of ATP but a sizeable proportion of axon boutons is devoid of mitochondria (Chavan et al., 2015; Pathak et al., 2015). At the post-synapse, one mitochondrion can span more than one dendritic spine such that local specificity is questioned (Delgado et al., 2019). Recent studies focused on local functions to clarify how the cost of synaptic plasticity distributes in dendrites (Devine and Kittler, 2018; Erturk et al., 2014; Rangaraju et al., 2019). Mitochondrial dysfunctions have emerged as cause or consequence of synaptopathies through mechanisms that could be synapse-specific (Lee et al., 2018).

A strong dependence on mitochondria could endanger neuronal activity and survival as an accumulation of mitochondrial damage could erode their functions (Picard et al., 2014). The more neuronal activity the higher is the energetic burden on mitochondria and synapses (Harris et al., 2012). A modeling study suggested that synaptic depotentiation is desirable for neuroprotection upon energy shortage (Bindokas et al., 1998). Synaptic scaling changes mitochondrial functions in response to varying states of excitation in epileptic as in ischemic tissues (Kirov et al., 2020; Rowley and Patel, 2013). Smaller mitochondria and lower levels of metabolites are hallmarks of adaptive plasticity to epileptic and ischemic events (Kislin et al., 2017). To this effect, the transient induction of metabolic stress immediate-early-genes like *Nr4a1*, a transcription factor for glycolysis and mitochondria components, is intended to adjust metabolism to synapse number (Jeanneteau et al., 2018; Zhang et al., 2009). Also, a shift between glycolytic and mitochondrial metabolisms reported during intense synaptic activity could be a mechanism to rapidly reduce oxidation and energy shortage (Sobieski et al., 2017). However, metabolic deficits and oxidative stress reported in

* Corresponding author.
E-mail address: freddy.jeanneteau@igf.cnrs.fr (F. Jeanneteau).

https://doi.org/10.1016/j.ynstr.2021.100402
Received 12 July 2021; Received in revised form 16 September 2021; Accepted 17 September 2021
Available online 21 September 2021

experimental and human neurodegeneration (Lin and Beal, 2006; Terada et al., 2020), and in stress-related neuropsychiatric disorders (Jeanneteau and Arango-Lievano, 2016; Picard et al., 2018) are associated with dysfunctions of such protective mechanisms.

Mitochondria are prime candidates to assume the energetic cost of synaptic plasticity to chronic unpredictable stress. However, many synapses lack proximal mitochondria raising questions about the subcellular distribution of this cost. Neurons are functionally polarized, exhibiting varying degree of activity along the dendritic tree that must transform into localized energy demands (Harris et al., 2012). Yet, the heterogeneity of cellular mitochondria is seldom addressed *in vivo* when studying dysfunction of mitochondria in the entire tissue or as a cellular pool. Studies of purified mitochondria from synaptosomes undermined the role of synapse heterogeneity (inhibitory versus excitatory, mature versus immature). Electron microscopy provided precise cytoarchitecture but lacks temporal resolution (Delgado et al., 2019). Real-time imaging revealed subcellular polarization and synapse-specific mitochondrial functions *in vitro* (Li et al., 2004; Rangaraju et al., 2019). However, mitochondria dynamics *in vitro* and *in vivo* are not alike in part due to development and the environment of experimental preparations (Faits et al., 2016). A majority of recent *in vivo* studies focused on pre-synaptic mitochondria in terminal experiments (Lee et al., 2018). The currently known mechanisms regulating post-synaptic mitochondria structure and function are based on *ex vivo* and *in vitro* experiments that do not reproduce local and global brain energy homeostasis (Natsubori et al., 2020).

Here, we imaged the *in-vivo* dynamics of dendritic spine turnover and mitochondrial function in pyramidal neurons of cortex at times of energy demands to capture the basal needs of homeostasis and the extra costs of adaptive plasticity to chronic unpredictable stress. We observed clusters of dendritic spine dynamics that associated with the remodeling of proximal mitochondrial coverage were greater than chance after chronic stress exposure. Functionally, less mitochondrial ATP production coupled with a loss of mitochondria and proximal dendritic spines after chronic unpredictable stress. And yet, fragmented mitochondria increased ATP production to keep up with acute excitation at the expense of higher H2O2 production. Given the previous implications of the orphan nuclear receptor NR4A1 in neuronal survival, mitochondria and dendritic spine number (Chen et al., 2014; Jeanneteau et al., 2018; Zhang et al., 2009), we used gain and loss of function experiments with recombinant and mutant forms of inducible NR4A1 to interrogate its role on the cross-remodeling of dendritic spines with mitochondria. Data indicated that neurons prepare to face future excitatory demands by distributing the burden of chronic stress through proximal remodeling of dendritic spines and mitochondria.

2. Methods

2.1. Animals

The French ministry of research and ethics committee CEEA36 approved the protocols adhering to the 2010/63/UE directive of the European community for the care and use of laboratory animals. All animals, CD1 mice (Janvier Labs, France) were allowed *ad libitum* access to food, water, and maintained on a 12-hr light-dark cycle unless indicated otherwise. The acute stress group received the same stressor (2-hr restrain) as the chronic stress group on the last day of the procedure. The chronic unpredictable stress procedure is as follows: lights on all day (Saturday), tilted cage and no bedding (Sunday), 6-hrs restrain (Monday), no food (Tuesday), forced swim test and flooded bedding overnight (Wednesday), crowded cage (Thursday), 2-hrs restrain (Friday). It was repeated for 2 weeks starting at 1 month of age. Such a chronic unpredictable and uncontrollable stress caused significant immobility in the tail suspension test and preference for the closed arms of the elevated plus maze at two distant time points (Fig. 3). Doxycycline (2 mg/ml, Clontech, Saint-Germain, France) was administered via the drinking water and refreshed every 5 days to induce the expression of transgenes with a Tet-ON system as previously described (Arango-Lievano et al., 2016b). Status epilepticus seizures induced by intraperitoneal injection of kainic acid (25 mg/kg, Sigma Aldrich) was previously described by us (Arango-Lievano et al., 2018) and causes focal cell death that served as positive control for comparison with the chronic stress. Males only were used in all procedures and deeply anesthetized before sacrifice with pentobarbital (50 mg/kg, i.p.). For molecular expression studies, cortical biopsies were punched out of fresh cold brain sections after the last imaging session and snap frozen in liquid nitrogen. For histology, mice were perfused with 4% ice-cold PFA.

2.2. In utero electroporation

Time-pregnant CD1 mice were utilized for *in utero* electroporation as previously (Arango-Lievano et al., 2016b) because the strain is highly sensitive to stress and the number of pups per litter allowed for less dams undergoing surgeries. Plasmid DNA encoding for Mito-roGFP-Orp1 and Mito-ATeam are described in (van Hameren et al., 2019), Mito-dsRed obtained from F. Saudou (GIN, Grenoble, France) is described in (Virlogeux et al., 2018), plasmids for doxycycline-dependent NR4A1, ΔAF1, R337A and GFP control are described in (Jeanneteau et al., 2018). One μg of plasmid DNA was injected in the ventricle at E15 on CD1 mouse embryos and electroporated (NEPA21, Nepagene, 30V, pON 50 msec, pOFF 950 msec, 5 pulses) as described (Jeanneteau et al., 2010). Mice were anesthesized with 4% isoflurane/oxygen and maintained at 1.5–2% isoflurane (Abbott laboratories, Chicago, IL) throughout surgery using TEC3N (Anesteo, Lunel, France). Mice received preemptive analgesia with Lidocaïne (Xylovet®, 3.5 mg/kg at incision site). A subcutaneous injection of the analgesic buprenorphine (Buprecare®, 0.05 mg/kg) was administered post-surgery and the next 3 days. Expression of transgenes in experimental animals generated by *in utero* electroporation was detected at 3 months of age in postmortem studies with immunohistology (Fig. 1C) but live fluorescence was too low for transcranial 2-photon microscopy at the latter time point. For this reason, we imaged cortex imaged *in vivo* tracers between 1 and 1.5 months of age.

2.3. Elevated plus maze

It is a typical test to measure anxiety in rodent models. The maze is at 50 cm above floor level in a room with dim light were mice were habituated for 45 min before testing. Mice were placed in the center and the entries and time spent in the open arms were visualized during the 5 min.

2.4. Tail suspension test

It is a typical test to measure behavioral motivation to escape inhospitable environment in rodent models. For habituation, the tail was taped 5 min before suspension to a hook located in a 56 × 40 × 33 cm box with dim light. Time of immobility postures was counted during 6 min. Slight movements of hindlimbs only were also considered as immobility.

2.5. Surgery and cranial window

Mice were anesthetized with a mix of 0.075 mg/g ketamine and 0.01 mg/g xylazine and lidocaine sprayed atop the skull prior to surgery. Skull bone was thinned between imaging sessions down to 18–20 μm thick using disposable ophthalmic surgical blades (Surgistar). The scalp is sutured and topped with antibiotic cream to avoid infection between imaging sessions 2 weeks apart. A detailed map of the pial vasculature was taken at macroscopic and microscopic scales for subsequent relocation between sessions. The second imaging session was performed on the day after exposition to the last stressor (day 14). Thinned-skull imaging was performed as previously described (Arango-Lievano et al.,

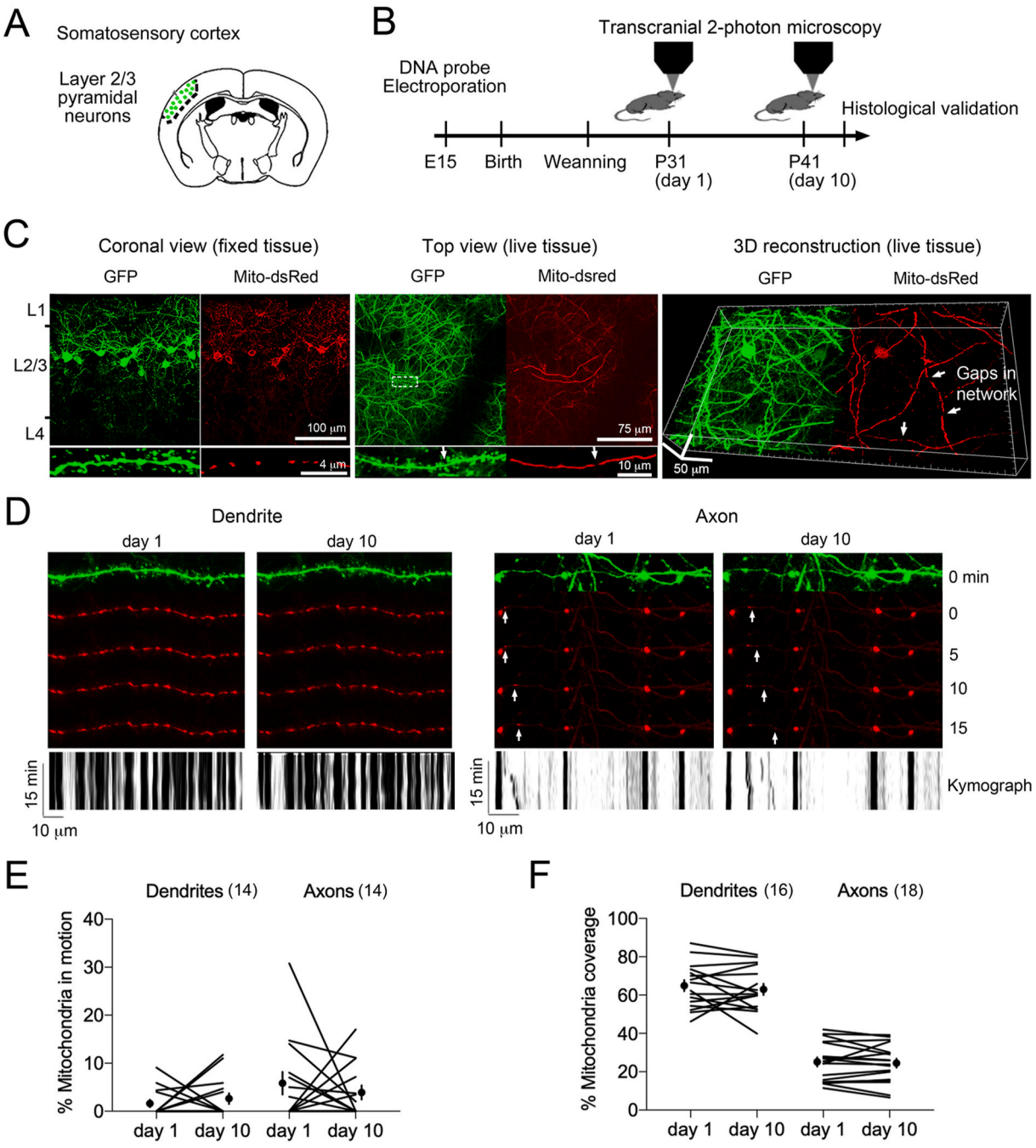

Fig. 1. The dendritic mitochondrial network is stable in the adult living cortex.

A. Fluorescent probes mito-dsRed and GFP targeted in pyramidal neurons of somatosensory cortex using *in utero* electroporation in mice.

B. Experimental timeline.

C. Imaging of fluorescent probes in fixed tissue section using confocal microscopy (left), in live tissue using transcranial two-photon microscopy (middle) and 3D reconstruction images using Imaris.

D. Time-lapse images of mitochondrial network twice 10 days apart reveals far less remodeling between time points in the dendrite (left) than in the axon (right) (see inset kymographs).

E. Proportion of mitochondria in motion during time lapse imaging of the same dendrites and axons between days, N = 14 segments each, 3 mice.

F. Proportion of mitochondria with coverage remodeling during time lapse imaging of the same dendrites and axons between days, N = 16 and 18 segments respectively, 3 mice. Two-way ANOVA for the dendritic vs axonal coverage of mitochondria $F_{1,32} = 128$ post-hoc Sidak test $p < 0.0001$.

2016a) and preferred to open skull preparation to avoid artifacts of surgical inflammation (Arango-Lievano et al., 2018). In terminal session, open-skull preparation was performed to deliver molecules locally as previously described (Arango-Lievano et al., 2019). A 3–4 mm craniotomy was prepared over the transcranial imaging zone and the underlying dura was removed and kept in an aqueous environment of HEPES-buffered artificial cerebrospinal fluid (ACSF in mM 120 NaCl, 3.5 KCl, 0.4 KH2PO4, 15 glucose, 1.2 CaCl2, 5 NaHCO3, 1.2 Na2SO4, 20 HEPES, pH = 7.4). The cortex was covered by a thin layer of low-melting agarose 1.5% in ACSF to avoid heartbeat motion artifacts. In order, ACSF was added through the agarose bed to capture baseline activity of fluorescent probes prior addition of glutamate (200 mM) slowly

diffusing from agarose to the cortex, followed by ACSF again and finally either Carbonyl cyanide-4-(trifluoromethoxy)phenylhydrazone (FCCP 10 μM a control for the Mito-ATeam probe) or H2O2 (10 μM, a control for the Mito-roGFP-Orp1 probe). Small molecules are from Sigma Aldrich (Saint-Quentin, France).

2.6. Image acquisition

Images were acquired with a FVMPE RS two-photon microscope (Olympus) equiped with a 25 ×, numerical aperture (NA) 1.05 water-immersion objective (XLPLN25XWMP2, Olympus) and an InSight X3 femtosecond-pulsed infrared laser (Spectra-Physics) for optimal fluorescence excitation and emission separation. Images were taken with a digital zoom of 7.2 at each image session using 0.75 μm step with a scanning dwell time of 2.55 μsec per pixel. Laser power was adjusted with the depth of imaging and kept below 50 mW. Time-lapse acquisition were done with galvanometric scanning mode and conventional raster scanning every 30 s for 5–10 min interspaced of 20 min during 1 h. Each image is a stack of scans over 20 μm depth. For Mito-dsred and GFP, a single track at 1040 nm excitation wavelength is used to obtain both GFP (em. 509 nm) and dsRed (em. 583 nm) images at the same time point. For ATeam, 850 nm excitation wavelength is used to obtain both CFP (em. 475 nm) and YFP (em. 527 nm) images at the same time point. For roGFP, the two images were acquired for each time point using alternating tracks 940 nm and 800 nm. Change of track was set after each stack. Each scan was obtained with constant laser intensity at 512 × 512 pixel resolution and microscope-imaging parameters were maintained between sessions.

2.7. Image analysis

The field of view (200 × 200 x 150 and 50 × 50 × 50 μm) was reconstructed with Imaris 8.0 (Bitplane) from z-stack images. Consecutive images were realigned with RegStack (ImageJ). Movie correction from movement due to respiration and blood pressure were done using Image stabilizer (ImageJ). Using ImageJ, we defined a region of interest encompassing the labeled dendritic mitochondria to measure the mean intensity on both images subtracted of background to calculate the ratio YFP/CFP for ATP levels and oxided/reduced roGFP for H2O2 and. Mito-ATeam and Mito-roGFP-Orp1 probes were prior validated *in vivo* (Lin et al., 2019; van Hameren et al., 2019). Resting levels of ATP andH2O2 are the means of 10-min period of image acquisition. The mobility of Mito-dsRed was determined in dendrites and axons using ImageJ plugin Kymograph. Spines and mitochondria were tracked manually along dendritic and axonal segments from 3D stacks of consecutive sessions using ImageJ. The mitochondria coverage was determined as Mito-dsRed/GFP signal ratio.

Mitochondria remodeling was determined ≤5 μm from a spine cluster that appeared or disappeared between consecutive imaging sessions. A dynamic cluster was defined as 2 or more additions/eliminations of dendritic spines ≤5 μm as previously described (Frank et al., 2018). Images of dendrites were acquired within 150 μm from the skull surface representing the apical dendrites of pyramidal neurons oriented in the plane axis of imaging zone with little z-projection. All clear headed-protrusions emanating laterally from the dendritic shaft were counted. The presence, loss and gain of spines were quantified across days for each segment. Distance measurement between spines was set at the base of the neck to the base of the next spine following the trace of the dendritic shaft.

The clustering ratio equals the number of spines in cluster divided by the total number of new spines added/eliminated between imaging sessions. The cross-clustered spine dynamic ratio equals the number of new spines added/eliminated ≤5 μm distance of mitochondrial remodeling in the same dendrite divided by the total number of newly dynamic spines in the full length of the same dendrite. The net change ratio equals the number of spine additions or mitochondrial dendritic coverage minus the number of spine elimination or mitochondrial dendritic coverage, expressed as percentage of day 1.

Simulations of the distance between the nearest added/eliminated spines were performed to test if the observed distance is different from chance level. For this, one dynamic spine was kept in its fixed position while the other dynamic spines were permutated randomly. This operation was repeated as many times as the number of dynamic spines. For each permutation, one spine of a cluster was randomly re-assigned to all possible spine positions on that dendritic segment keeping the other spine in its fixed observed position. We used a Matlab code provided by Dr. Li Zuo and Dr. J. Lu (at Univ of California SC, USA) to measure the distance between the clustered spines for each permutation and repeated the process 30,000 times as previously (Chen et al., 2018; Fu et al., 2012). Averaged values yielded a random distribution of any possible spine clusters in defined dendritic territories from which we calculated the Gaussian Best-fit value (Mean ± SEM) to which we compared the experimentally observed value. We wrote a new Matlab code to run the simulations of the distance between the nearest dynamic spines and mitochondrial remodeling, again to test if the observed distance is different from chance level. For each permutation, one spine of a cluster was randomly re-assigned to all possible spine positions on that segment without changing mitochondrial remodeling from the observed position. The distance of each clustered spine to its nearest mitochondrial remodeling was measured. These values for each permutation from 30,000 simulations were averaged between animals. This yielded a random distribution of clustered spines on dendritic segments that is dependent of mitochondria remodeling from which we calculated the Gaussian Best-fit value (Mean ± SEM) to which we compared the experimentally observed value.

2.8. Cell culture

Primary E18 cortical neurons were prepared from time-pregnant Sprague Dawley rats (Janvier Labs, France), cultured for 3 weeks on glass coverslips coated with poly-D-lysine, and maintained in Neurobasal medium containing B27 supplement, 0.5 mM L-glutamine, 5-fluorouridine and uridine (10 μM each) (Life Technologies, Carlsbad, CA). Cells were transfected with Lipofectamine 2000 (Life Technologies, Carlsbad, CA, USA) one week after plating for qualitative experiments or electroporated immediately after dissection with the AMAXA system for qPCR and luminescence analyses. Doxycycline (10 ng/ml, 3 h) from Clontech (Saint-Germain, France) was used to induce NR4A1 expression. Corticosterone (10 μM, 3 h) from Sigma Aldrich (Saint-Quentin, France) was used to trigger endogenous NR4A1 expression.

2.9. RNA extraction and quantitative PCR

TRIzol (ThermoFisher Scientific, Villebon sur Yvette, France) was used to extract total RNA tissue homogenates as well as primary neurons. cDNA was synthesized from 1 μg of RNA using the First-Strand cDNA Synthesis Kit for Real-Time PCR (USB, ThermoFisher Scientific, Villebon sur Yvette, France) and random primer mix (USB, ThermoFisher Scientific, Villebon sur Yvette, France). Hot-start SYBR Green PCR kit (Qiagen France SAS) was used in 10 μL reactions containing 2.5 μL of cDNA, and 100 nM primers mix. Rodent specific primers are as follow (5′ to 3′): *drp1* TGATGGGAAGGGTTATTCCA and TGGCCAGAGATGGGTACTTC; *mfn1* TCGCAGTCAGCAGTGAAAAC and TGCCACGTTTACTGAGTCCA; *mfn2* AGGAAATTGCTGCCATGAAC and TGTTGAGTTCGCTGTCCAAC; *opa1* GGACCCAAGAGCAGTGTGTT and GGTTCTTCCGGACTGTGGTA; *fis1* GCCTGGTTCGAAGCAAATAC and CACGGCCAGGTAGAAGACAT; *ucp2* ACAAGACCATTGCACGAGAG and ATGAGGTTGGCTTTCAGGAG; *ucp4* TCTCACAAAAACCCGACTCC and ACCATCCGACCTCCAGAGTA; *ucp5* GGAATGCTGGGAGACACAAT and GTCCCACTATTGCCCTCTGA; *nr4a1* AGGACTTTCAGGTGTATGGCTGCT and AGTGGCCAAATGAACCATCCCAAG; and control genes *gapdh* CCTGCACCACCAACTGCTTAG and CTGTGGTCATGAGCCCTTCC; *rpl19*

CACAAGCTGAAGGCAGACAA and GCGTGCTTCCTTGGTCTTAG. Q-PCR was performed with ABI 7900 instrument (Applied Biosystems, France), followed by melt-curve analysis. Fold changes in gene expression were calculated using ΔΔCt (Ct = cycle number at threshold) analytical method that includes normalization against house-keeping genes *Gapdh and Rpl19*.

2.10. NR4A1 transcriptional activity

Plasmids encoding for NurRE-luc or NBRE-Luc and renilla (10:1 ratio) were electroporated with the AMAXA system in primary neurons further grown for a week *in vitro*. Luminescence emission was captured from cleared cell extracts (100 μg) using the Dual luciferase reporter assay according to manufacturer's instructions (Promega France). Data are expressed as a ratio of Luciferase/Renilla luminescence intensities.

2.11. Immunofluorescence

Brains were harvested and post-fixed for 2 h and equilibrated in 30% sucrose (Sigma Aldrich, Saint-Quentin, France). Free-floating coronal sections rinsed in PBS were blocked in 5% normal goat serum, PBS, 0.1% triton X-100 for 2 h at 25 °C. Primary antibodies, GFP 1:3,000 (Abcam, Cambridge, UK), NR4A1 E6 1:400 (Santa Cruz Biotechnology, Dallas, USA), RFP 1:2,000 (Rockland Immunochemicals, Limerick, PA), cleaved caspase-3 1:100 (Cell Signaling Technologies) were incubated for 2 days at 4 °C and secondary antibodies (ThermoFisher Scientific, Villebon sur Yvette, France 1:2,000) for 2 h at 25 °C. Cultured cells were fixed in 4% PFA, 20% sucrose in PBS for 10 min at 25 °C. After quenching the fixative with 50 mM NH_4Cl in PBS, cells were permeabilized with 0.1% triton X-100 in PBS for 3 min, blocked with 5% goat serum, 2% BSA and 0.25% fish skin gelatin in TBS for 30 min and then incubated with antibodies for 3-hrs in blocking solution at room temperature. Cells were washed in TBS, 0.25% fish skin gelatin and mounted in Mowiol (Sigma Aldrich, Saint-Quentin, France). Fluorescence images were taken on LSM780 laser-scanning confocal microscope (Carl Zeiss, Iena, Germany) equipped with x63 Plan-Neofluor NA1.3 oil-immersion objective. Z-stack images were processed using ImageJ.

2.12. Statistics

Data are shown as means ± standard error of the mean. Statistical significance was set at $p < 0.05$. Data were compared using two-tailed T-test (Student, Mann-Whitney), correlated with Pearson r for comparing 2 sets of variables or ANOVA to compare multiple groups followed by *post-hoc* pairwise comparison (Prism 8.0). For *in vivo* experiments, about 200 dendritic spines from at least 10–20 dendritic segments were counted per conditions throughout the imaging sessions and averaged per animal. For *in vitro* experiments, the number of culture dishes per group was equivalent to the number of independent experiments. For q-PCR experiments, samples were assessed in triplicates, averaged and pooled by groups of animals or culture dishes. Estimates of sample size were calculated based on previous studies and preliminary data. Animals and culture dishes were attributed to various experimental groups in a random fashion. All data collected in animals were from littermate controls and averaged per experimental groups. Data are deposited on 4TU.researchData repository.

3. Results

3.1. Time-lapse imaging of synaptic mitochondria in the living cortex

To track mitochondria and synapses in the living brain, we electroporated Mito-dsRed and eGFP during corticogenesis to target layer 2/3 pyramidal neurons in somatosensory cortex (Fig. 1A) due to its responsiveness to external stressors (Arango-Lievano et al., 2016b). After weaning, males were reared in groups living in standard conditions, and transcranial two-photon microscopy of probes started at 1 month-of-age (Fig. 1B) then repeated 10 days later in the same zone. Images revealed the gaps interspacing the mitochondrial network along dendritic territories (Fig. 1C).

Time-lapse imaging indicated that large mitochondria are stationary in their compartment while a minority of small ones moved between large ones within distances superior in axons than dendrites. At resting state, the coverage of mitochondrial network was stable, higher in dendrites than axons (Fig. 1D–F).

To assess the *in vivo* remodeling capacity of the mitochondrial network, we performed a craniotomy atop the somatosensory cortex of adult mice to apply locally the excitatory neurotransmitter glutamate (Fig. 2A and B). There was no indication of neurotoxicity in response to the high concentration of glutamate diffusing through the agarose bed of the craniotomy (Fig. S1). Real-time imaging upon injection of artificial cerebrovascular fluid (ACSF) revealed rare clumping and fragmenting events of the mitochondrial network (Fig. 2C and D). The following application of glutamate significantly reduced the mitochondrial network coverage in dendrites (Fig. 2G and H) with little impact on the proportion of mitochondria in motion (Fig. 2E and F).

In a third series of experiments, we used a transcranial window to image the same cortical territories twice, 14 days apart, before and after exposure to acute or chronic stressors that we compared with a group of unstressed controls (Fig. 3A). Specifically, the chronic unpredictable stress protocol of 2 weeks during adolescence (see methods for details) caused behavioral immobility in the tail suspension test (Fig. 3B) and preference for the closed arms of the elevated plus maze at two distant time points (Fig. 3C) as previously suggested (Yohn and Blendy, 2017). Images show a reduction of mitochondrial coverage in dendrites of chronically stressed mice that is not observed in the other groups (Fig. 3D and E). This is consistent with the loss of dendritic spines previously described in postmortem fixed tissues with the same stress protocol (Arango-Lievano et al., 2015). Together, both dendritic spines and mitochondria could evolve from stationary to dynamic states in times of stress.

3.2. Remodeling of the mitochondrial network at hotspots of dendritic spine turnover

Using the same methodology, we performed a new series of experiments with the chronic unpredictable stress protocol (Fig. 4A) that revealed significant decrease of new dendritic spine formation (−73 ± 9%, $p < 0.05$) and increase of pre-existing spine loss (+101 ± 21%, $p < 0.05$ Fig. S1) in agreement with a previous study in motor cortex (Arango-Lievano et al., 2019). To address the possibility of reciprocal structural dynamics between mitochondria and dendritic spines (Fig. 4B), we tracked the topography of additions and eliminations (Fig. 4C) presented schematically along dendritic territories (Fig. 4D). We postulated that (i) the turnover of dendritic spines in groups would more likely associate with the remodeling of proximal mitochondria than ungrouped dynamic spines, (ii) spine additions would associate with mitochondrial gain of coverage, (iii) spine eliminations would associate with mitochondrial loss of coverage. Using these criteria, we defined a distance ≤5 μm between the nearest added or eliminated spines to identify clusters as previously described (Frank et al., 2018; Takahashi et al., 2012). We use the terminology dendritic spine clustering as the product of 2 or more events within ≤5 μm and cross-clustering when 2 or more proximal spine dynamic events coincided with mitochondrial remodeling within the same perimeter. Both are quantified as the number of clustered spines divided by the total number of dynamic spines along dendrites (Clustering) or restricted to the perimeter of the dendrites with mitochondrial remodeling (Cross-clustering).

A simulation of the distance between the nearest added or eliminated spines was performed to test if the observed distance is different from chance level. For this, one dynamic spine was kept in its fixed position

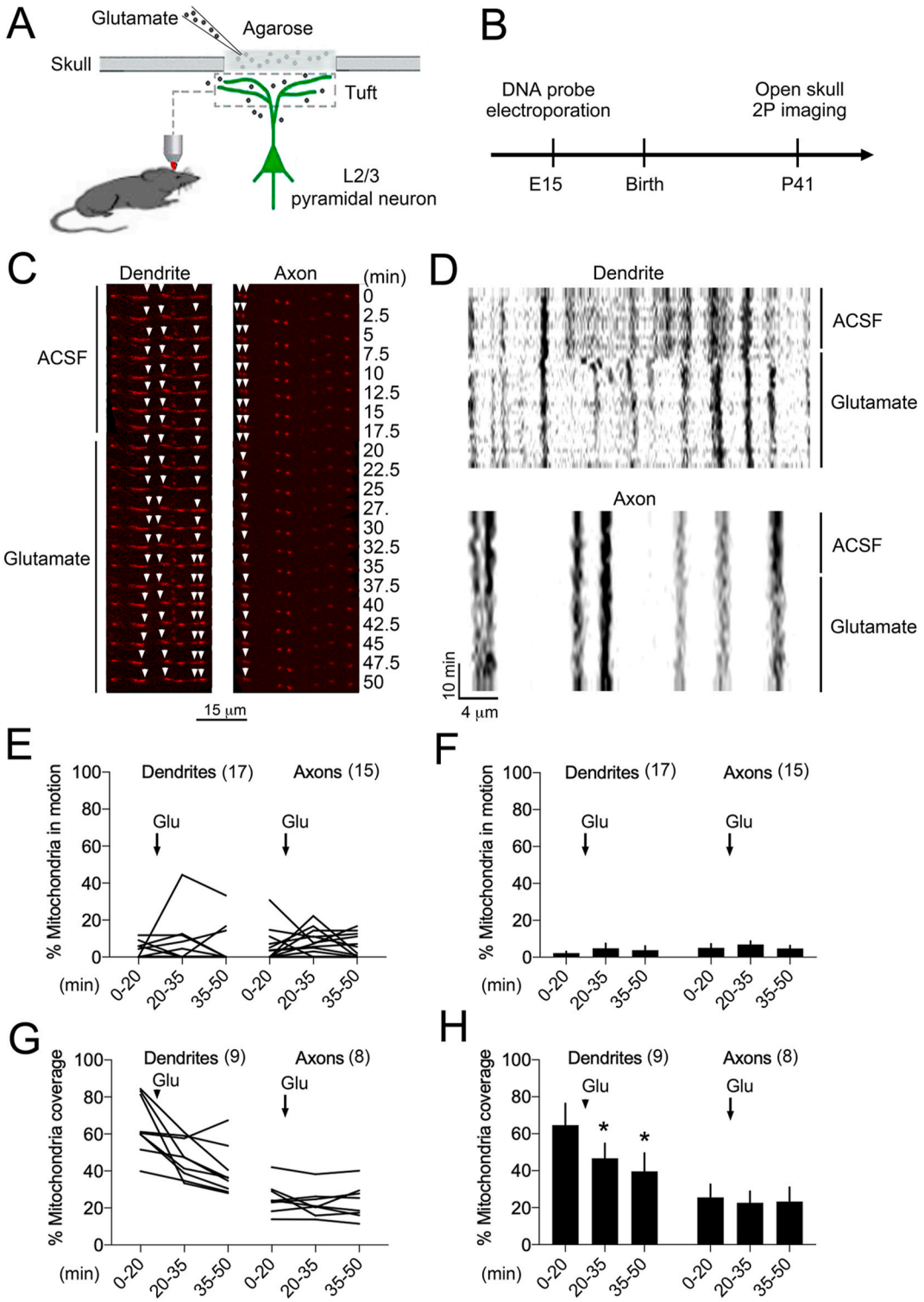

Fig. 2. Remodeling of the mitochondrial network after focal application of glutamate on cortex.

A. Time-lapse images of mito-dsRed in the axon and dendrites of pyramidal neurons of cortex before and after local application of 200 µM glutamate through a craniotomy. Arrows point to the remodeling events of the mitochondrial network.

B. Kymographs representing the clumping and fragmenting of the mitochondrial network.

C. Effect of glutamate on the proportion of mitochondrial coverage remodeling in dendrites and axons, N = 17 and 15 segments respectively, 3 mice.

D. Group data, one-way ANOVA in dendrites $F_{2,32} = 0.63$, $p > 0.5$ and axons $F_{2,28} = 0.63$, $p > 0.5$.

E. Effect of glutamate on the proportion of mitochondria in motion in dendrites and axons, N = 9 and 8 segments respectively, 3 mice.

F. Group data, one-way ANOVA $F_{2,16} = 12.27$, $p = 0.0006$ post-hoc Dunnett test comparing baseline and glutamate periods for dendrites $^*p = 0.0006$.

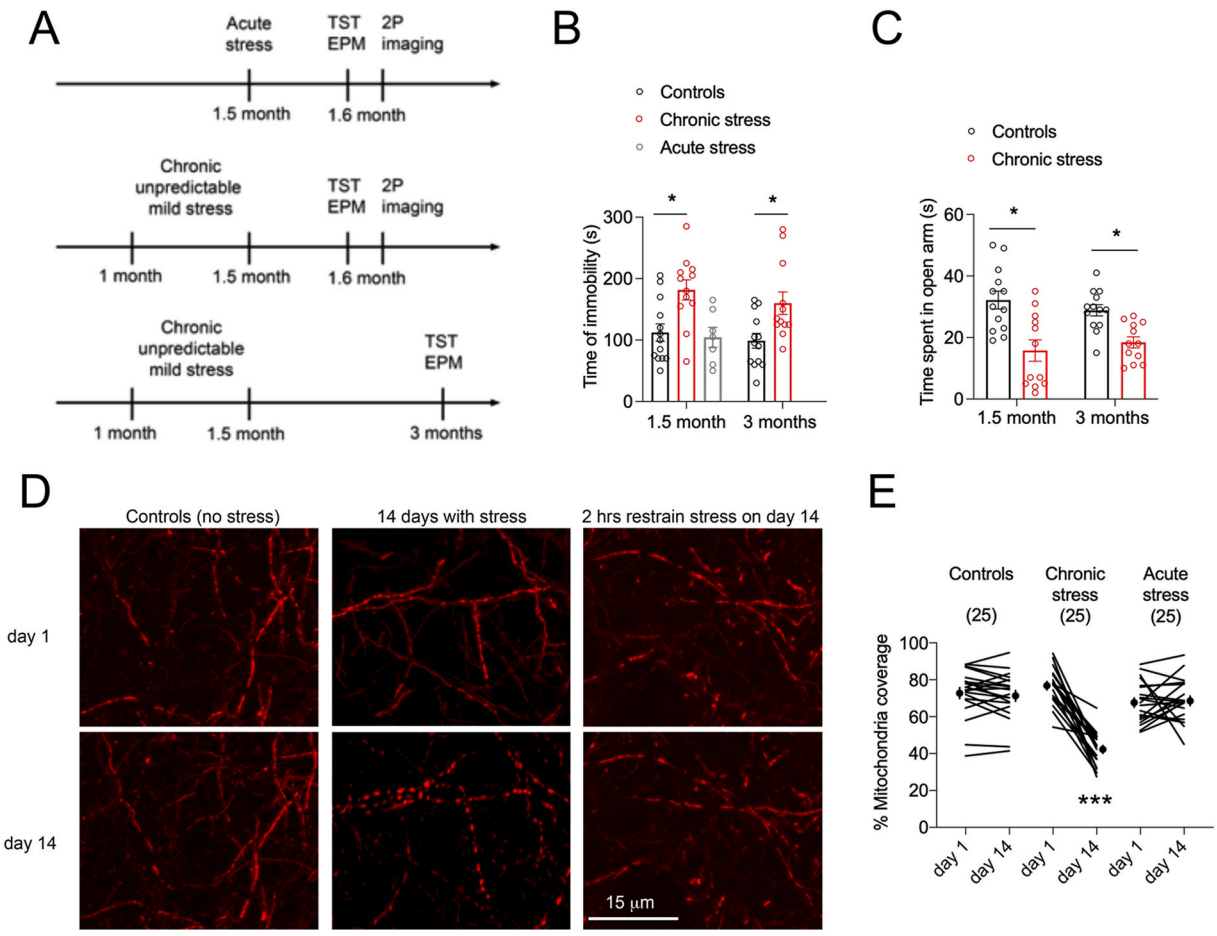

Fig. 3. Chronic unpredictable stress caused cortical remodeling of the mitochondrial network and behavioral impairment.

A. Experimental timelines.

B. Time of immobility in the tail suspension test (means ± SEM of N = 13 controls, 12 chronic stress, 7 acute retrain stress). One-way ANOVA: $F(4,52) = 5.73$ $p = 0.0007$, post-hoc Sidak test $^*p < 0.05$.

C. Time spent in the open arm of the elevated plus maze (means ± SEM of N = 13 controls, 12 chronic stress). Two-way ANOVA: $F(1,46) = 5.73$ $p = 0.0007$, post-hoc Tukey test $^*p < 0.05$.

D. Two-photon images of Mito-dsRed in cortex of mice before and after exposure to chronic unpredictable stress (14 days) or acute stress (2-hrs of restrain as the last stressor of the chronic stress protocol).

E. Effect of stress procedures on the proportion of mitochondrial coverage remodeling in dendrites. Student two-tailed T-test comparing day 1 and 14 in controls $p = 0.29$ and in stress groups $^{***}p < 0.0001$ and $p = 0.77$ respectively, N = 25 dendrites each, 4 mice per group.

while the other dynamic spines were randomly re-assigned to all possible spine positions on that dendritic segment. Spine permutations were repeated a total of 30,000 times to yield a random distribution of clustered spines to which we compared the experimental value. Data indicated that chronic stress triggered clustered spine dynamics that is different from chance ($p < 0.05$, Fig. 4E). Additional simulations were then performed to determine if spine clustering and mitochondrial remodeling covariate beyond chance level. For each permutation, one spine of a cluster was randomly re-assigned to all possible spine positions on that segment without changing mitochondrial remodeling from the observed position. The distance of each clustered spine to its nearest mitochondrial remodeling was measured and averaged between animals. Spine permutations were repeated a total of 30,000 times to yield a random distribution of clustered spines on dendritic segments that is dependent of mitochondria remodeling. Data indicate that the observed cross-clustering of dendritic spines with proximal mitochondria is also greater than chance ($p < 0.05$, Fig. 4F).

As chronic stress shifted to more clustered spine loss (+84 ± 14%, $p < 0.05$ Fig. 4G) than gain (−68 ± 10.9%, $p < 0.05$, Fig. 4G), the mitochondrial coverage was reduced within spine clusters (−73 ± 12% for additions and +88 ± 8.4% for losses, $p < 0.05$, Fig. 4H). Overall, there was a net loss of dendritic spines and mitochondrial coverage in the chronic stress group but no net change in the control group (−18.9 ± 3% for mitochondria and −10.4 ± 1.5% for spines, $p < 0.05$, Fig. 4I), which correlated within animals and between groups ($p < 0.05$, Fig. 4J).

3.3. *Chronic stress alters the resting and excited states of dendritic mitochondrial function*

To investigate the physiology of fragmented mitochondria, we introduced functional probes in pyramidal neurons of somatosensory cortex for real-time imaging before and after stress. We used two different probes: Mito-ATeam based on Förster resonance energy transfer (FRET) to detect ATP in mitochondrial matrix (Yoshida et al., 2017). ATP binding causes reversible conformational change, eliciting FRET transfer between CFP and YFP domains. Relative ATP levels are measured with the YFP/CFP fluorescence ratio (Fig. S3). Mito-roGFP-Orp1 based on redox sensitive GFP reversibly shifts from reduced to oxidized forms to detect H2O2 in mitochondrial matrix (Albrecht et al., 2011). Relative H2O2 levels are measured with oxidized/reduced ratio of emitted fluorescence (Fig. S4).

At first, we investigated changes of FRET ratio over 10-min period in

the same dendritic territories (Fig. 5A,D) before and after chronic stress. While no change occurred in resting conditions, mitochondrial ATP level was significantly decreased in chronic stress conditions (−24 ± 5.7%, $p < 0.05$, Fig. 5A and B). Levels of mitochondrial H202 were not altered in these conditions (−3 ±2% Fig. 5D and E).

Second, a craniotomy capped with agarose atop the imaging zone to avoid motion artifacts allowed infusions of artificial cerebrospinal fluid for baseline measures and glutamate for the evoked measures. FCCP, a mitochondrial protonophore that quenches ATP synthesis, was used as control for MitoAteam. H2O2 was used as control for Mito-roGFP-Orp1. In control animals, ATP levels increased (+9.9 ± 0.4%, $p < 0.05$, Fig. 5C), H202 levels did not change (−2.7 ± 0.9% Fig. 5F) when neurons were stimulated with glutamate indicating the mitochondrial buffering capacity of the oxidative stress while producing ATP in time of

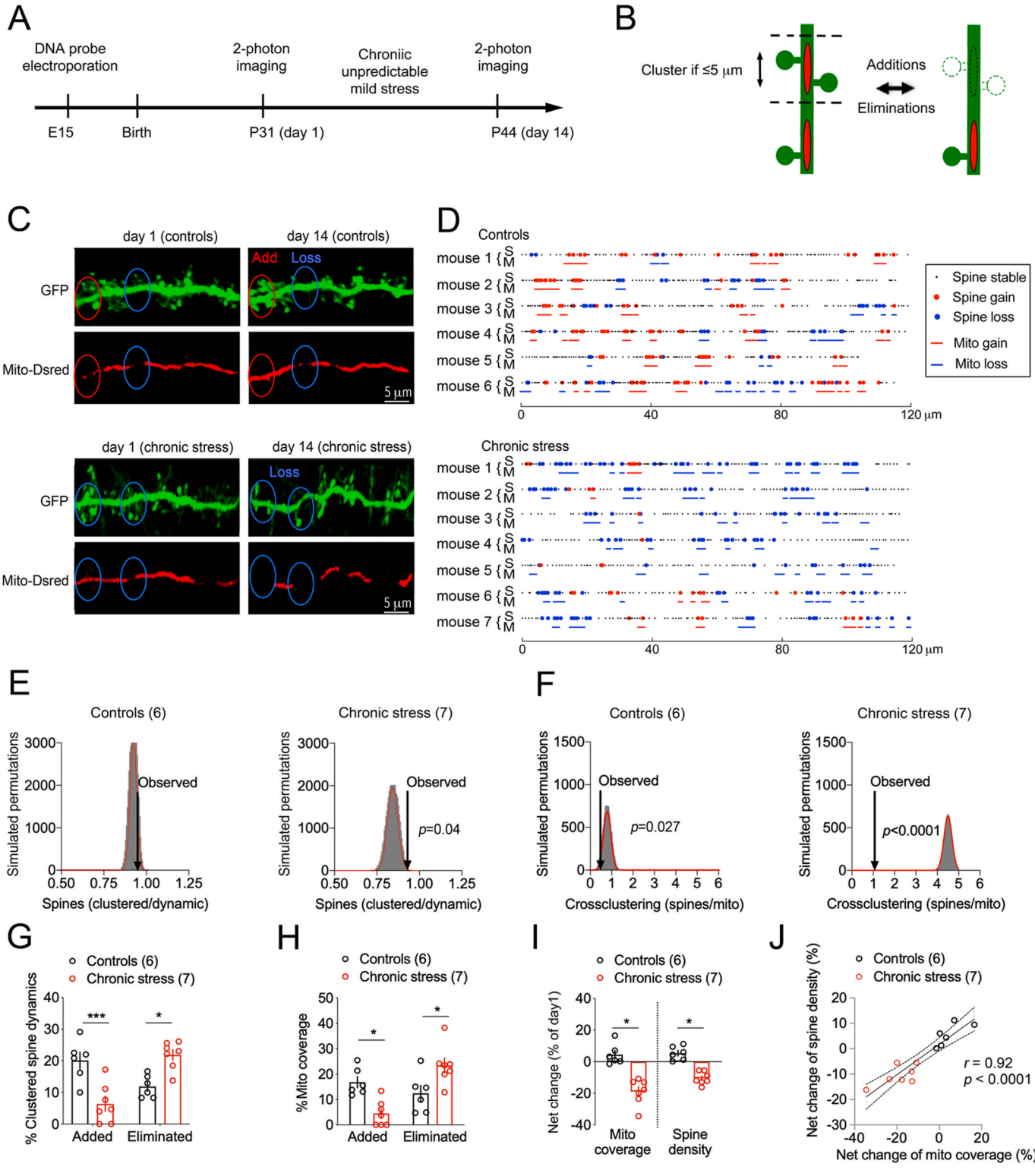

(caption on next page)

Fig. 4. Mitochondrial network remodeling at sites of dendritic spine turnover.
A. Experimental timeline.
B. Working model.
C. Two-photon images of dendritic Mito-dsRed and GFP in pyramidal neurons of cortex before and after chronic stress. A distance ≤5 μm is indicated where the loss/gain of groups of spines corresponded with the loss/gain of mitochondrial coverage.
D. Topography of mitochondria (M) and spine (S) remodeling in dendritic territories imaged twice 14 days apart.
E. Clustered spine dynamics is greater than chance. Histogram shows the distribution of spine permutations in 30,000 simulations of randomized new spine positions (mean Gaussian fit = 0.94 ± 0.014, observed = 0.97 ± 0.35, N = 6 Controls, $p = 0.1$ and mean Gaussian fit = 0.84 ± 0.03, observed = 0.93 ± 0.1, N = 7 Stress, $p = 0.04$).
F. Cross-clustering of proximal (≤5 μm) spine dynamics and mito remodeling is greater than chance. Histogram shows the distribution of spine permutations in 30,000 simulations of randomized new spine positions with respect to mito remodeling (mean Gaussian fit = 0.786 ± 0.17, observed = 0.58 ± 0.075, N = 6 Controls, $p = 0.027$ and mean Gaussian fit = 4.5 ± 0.18, observed = 1.02 ± 0.37, N = 7 Stress, $p < 0.0001$).
G. Gain/loss of clustered dendritic spines. Two-way ANOVA: stress x clustered dynamic $F_{1,22} = 32.45$, $p < 0.0001$ post-hoc Tukey test: control vs stress groups for gains $p = 0.0007$ for losses $p = 0.012$, N = 7 stress, 6 control mice.
H. Gain/loss of dendritic mitochondrial coverage. Two-way ANOVA: stress x mitochondrial remodeling $F_{1,22} = 20.37$, $p = 0.0002$ post-hoc Tukey test: control vs stress for gains $p = 0.013$ for losses $p = 0.03$, N = 7 stress, 6 control mice.
I. Effect of stress on the net change of mitochondrial coverage and spine density. Student two-tailed T-test comparing control and stress groups for the mitochondria $^*p = 0.0005$ and spines $^*p = 0.001$, N = 7 stress and 6 control mice.
J. Pearson correlation between the net change of spine density and mitochondria coverage.

demands. In stressed animals, ATP production (+34 ± 2.3%, $p < 0.05$) was correlated with a significant increase of H202 (+21.9 ± 1.46%, $p < 0.05$), indicating that oxidative stress was also increasing in active dendrites. The effects of chronic stress could rely on local elevation of extracellular glutamate that is sufficient to fragment dendritic mitochondria.

Together, the results indicate that mitochondrial ATP production is flexible in the dendrites of chronically stressed animals, transitioning from a new lower set point at rest to a higher peak of activity upon excitatory challenge that coincided with deregulated oxidation output.

3.4. Transcriptional programming of mitochondrial plasticity to stress

To investigate the mechanism of mitochondrial plasticity to stress, we harvested postmortem biopsies of the imaging zone and assessed the expression levels of mitochondrial markers previously involved in neuronal health, plasticity and stress-related diseases. In particular, the fission/fusion pathway keeps mitochondria healthy while the

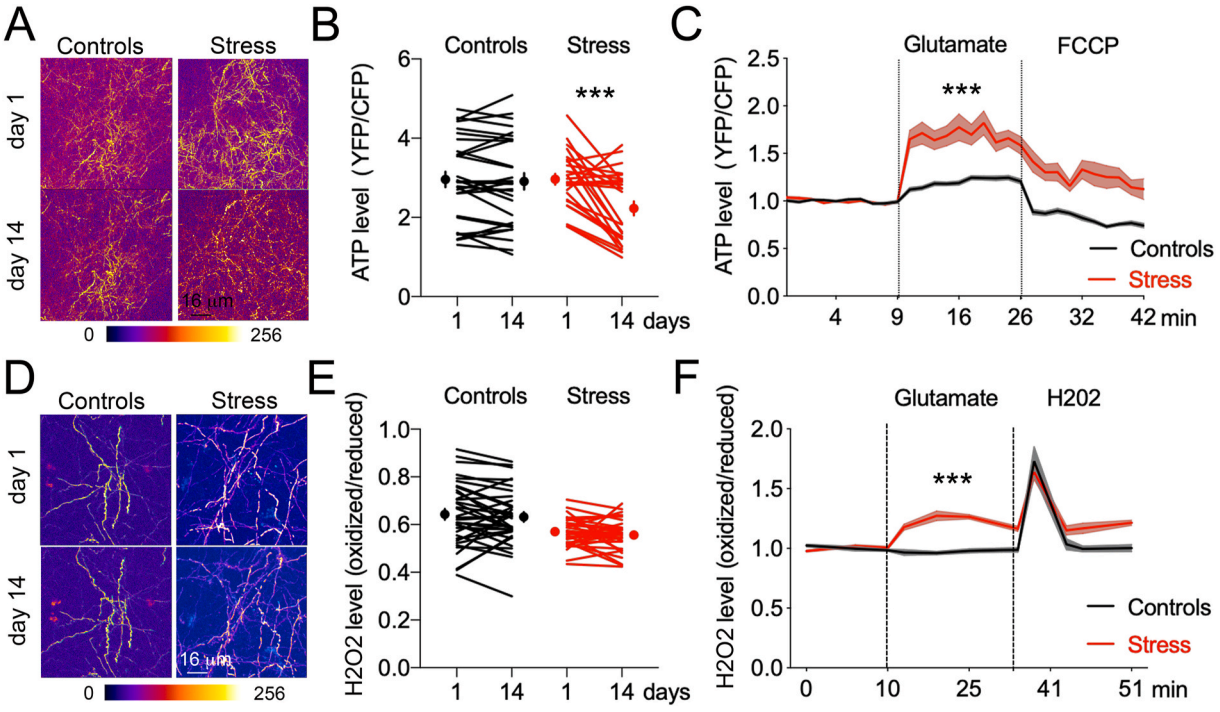

Fig. 5. Mitochondrial ATP and H2O2 levels before and after chronic stress.
A. Time-lapse images of Mito-ATeam fluorescence ratio in the same dendritic territories.
B. Mitochondrial ATP levels in resting state. Student two-tailed T-test: day 1 vs 14 for controls $p = 0.41$ for stress $^{***}p = 0.0022$, N = 26 control, 29 stress dendrites, 5 mice/group.
C. Mitochondrial ATP levels on day 14 after application of 200 μM glutamate and 10 μM FCCP on cortex via a craniotomy. Two-way ANOVA: time x stress $F_{29,3802} = 11.57$, $p < 0.0001$ post-hoc Sidak test: control vs stress $^{***}p < 0.0001$, N = 68 control, 71 stress dendrites, 5 mice/group.
D. Time-lapse images of Mito-roGFP-Orp1 fluorescence ratio in the same dendritic territories.
E. Mitochondrial H2O2 levels in resting state. Student two-tailed T-test: day 1 vs 14 for controls $p = 0.41$ for stress $p = 0.23$, N = 35 control, 33 stress dendrites, 4 mice/group.
F. Mitochondrial H2O2 levels on day 14 after application of 200 μM glutamate and 10 μM H2O2 via a craniotomy. Two-way ANOVA: time x stress $F_{10,430} = 7.2$, $p < 0.0001$ post-hoc Sidak test: control vs stress $^{***}p < 0.0001$, N = 22 control, 23 stress dendrites, 4 mice/group.

uncoupling proteins modulate the proton gradient and the level of oxidation (Devine and Kittler, 2018; Mattson et al., 2008). Quantitative analysis of mRNA levels for a selection of genes in these pathways helped to profile how acute stimulation with glutamate and chronic stress could result in fragmentation and metabolic alterations. The response to glutamate was different between the stress and control groups for the expression of *Fis1*, *Mfn1* and *Ucp4*. Notably, chronic stress caused a switch of expression between *Ucp2* ($-77.2 \pm 14.9\%$, $p < 0.05$) and *Ucp4* ($+57.5 \pm 26.3\%$, $p < 0.05$) that remained upon acute excitation with glutamate (Fig. 6A). Changes of *Ucp2*:*Ucp4* ratio was previously linked to the Warburg effect for explaining fuel utilization during cell fate transition in cancer cells and Parkinson's disease (Ayyasamy et al., 2011; Chu et al., 2009; Liu et al., 2006; Rupprecht et al., 2014).

We thought to exploit the *Ucp2*:*Ucp4* ratio as a marker of the adaptive response to neuronal stress and search for regulatory genes. To this end, we cultured pyramidal cortical neurons derived from mouse embryos because they can be transfected by electroporation with high efficiency. Transfection with the recombinant orphan nuclear receptor NR4A1 altered the *Ucp2*:*Ucp4* ratio like did chronic stress and glutamate excitation ($-52.9 \pm 8.3\%$ for *Ucp2 and* $+ 81 \pm 38.8\%$ for *Ucp4*, $p < 0.05$ Fig. 6B). In contrast, transfection of a NR4A1 mutant lacking transcriptional abilities produced significantly different results ($+88.6 \pm 50.5\%$ for *Ucp2 and* $-6.9 \pm 51.7\%$ for *Ucp4*, $p < 0.05$). Previous study reported that NR4A1 expression increased with neuronal depolarization, glutamate stimulation (Chen et al., 2014). Here we used corticosterone stimulation of cultured cortical pyramidal neurons to show that NR4A1 expression was significantly induced by a stress hormone ($+387.7 \pm 47.6\%$, $p < 0.05$, Fig. 6C).

3.5. Promoting the loss of dendritic spines and mitochondria hotspots

To test whether NR4A1 contributes to the turnover of dendritic spine clusters and proximal mitochondria, we used a pharmacogenetic approach to induce its expression with doxycycline (dox) (Fig. 7A, Fig. S5). NR4A1 construct was electroporated with Mito-dsRed in cortex, and two-photon images acquired 14 days apart ± dox in the drinking water (Fig. 7B). The topography of dendritic spines and mitochondria additions/eliminations significantly changed between the ON and OFF dox groups (Fig. 7C). Comparison between the observed and simulated dynamic events indicated that spine clustering and cross-clustering with proximal mitochondria are also greater than chance in these conditions ($p < 0.05$, Fig. 7D and E). Dox exposure promoted more elimination (the clustered $+176.6 \pm 7.3\%$, $p < 0.05$, Fig. 7F versus the total $+144.9 \pm 26.8\%$, $p < 0.0001$, Fig. S6A) than gain of spines (the clustered $-36.1 \pm 12.6\%$, $p < 0.05$, Fig. 7F versus the total $+84 \pm 14\%$, $p = 0.1$, Fig. S6A), and more elimination of mitochondrial coverage ($+395 \pm 17\%$ for losses and -31.5 ± 17 for gains, $p < 0.05$, Fig. 7G). Dox treatment resulted in a net loss of spine number ($-11.9 \pm 0.9\%$, $p < 0.05$) and mitochondrial coverage ($-34 \pm 7.7\%$, $p < 0.05$, Fig. 7H), which correlated between animals and groups (Fig. 7I). Results suggest that ectopic prolonged expression of NR4A1 mimicked the structural effects of chronic stress on dendritic mitochondria.

3.6. Preventing the loss of dendritic spines and mitochondria hotspots

To block NR4A1 activity, we expressed dox-dependent mutants that lack transcriptional abilities and did not interfere with dendritic mitochondrial coverage and spine density in pyramidal neurons of

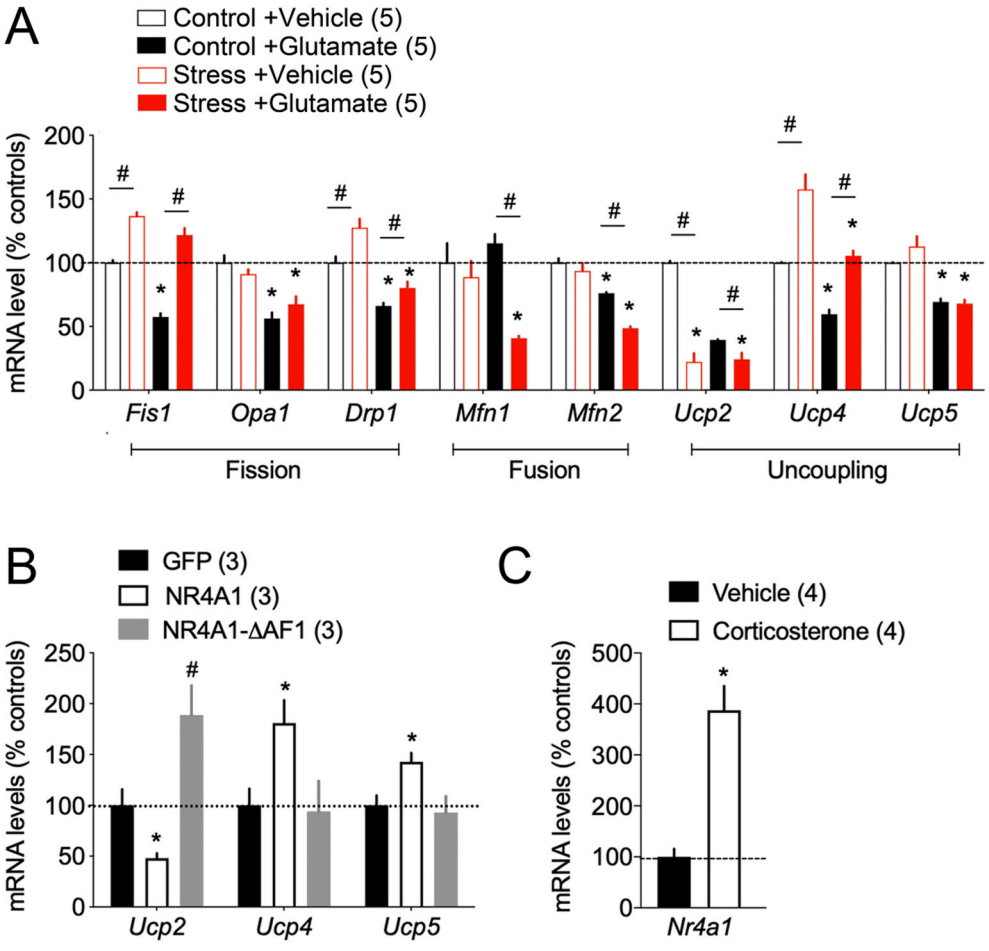

Fig. 6. Expression of mitochondria regulatory genes sensitive to stress and glutamate.
A. Interaction of glutamate application (200 μM, 60 min) via a craniotomy and chronic stress (14 days) on indicated mRNA levels in somatosensory cortex. Student two-tailed T-test: controls vs stress for vehicle $^{\#}p < 0.05$ for glutamate $^{*}p < 0.05$, N = 5 mice/group.
B. *Ucp* mRNA levels after induction of the metabolic gene *Nr4a1* and dominant-negative ΔAF1 in cortical neurons. Mann-Whitney two-tailed T-test: NR4A1 vs GFP $^{*}p < 0.05$, NR4A1 vs ΔAF1 $^{\#}p < 0.05$, N = 3 experiments.
C. *Nr4a1* mRNA levels after stimulation of cortical neurons with 10 μM Corticosterone for 3-hrs. Mann-Whitney two-tailed T-test: vehicle vs corticosterone $^{*}p < 0.05$, N = 4 experiments.

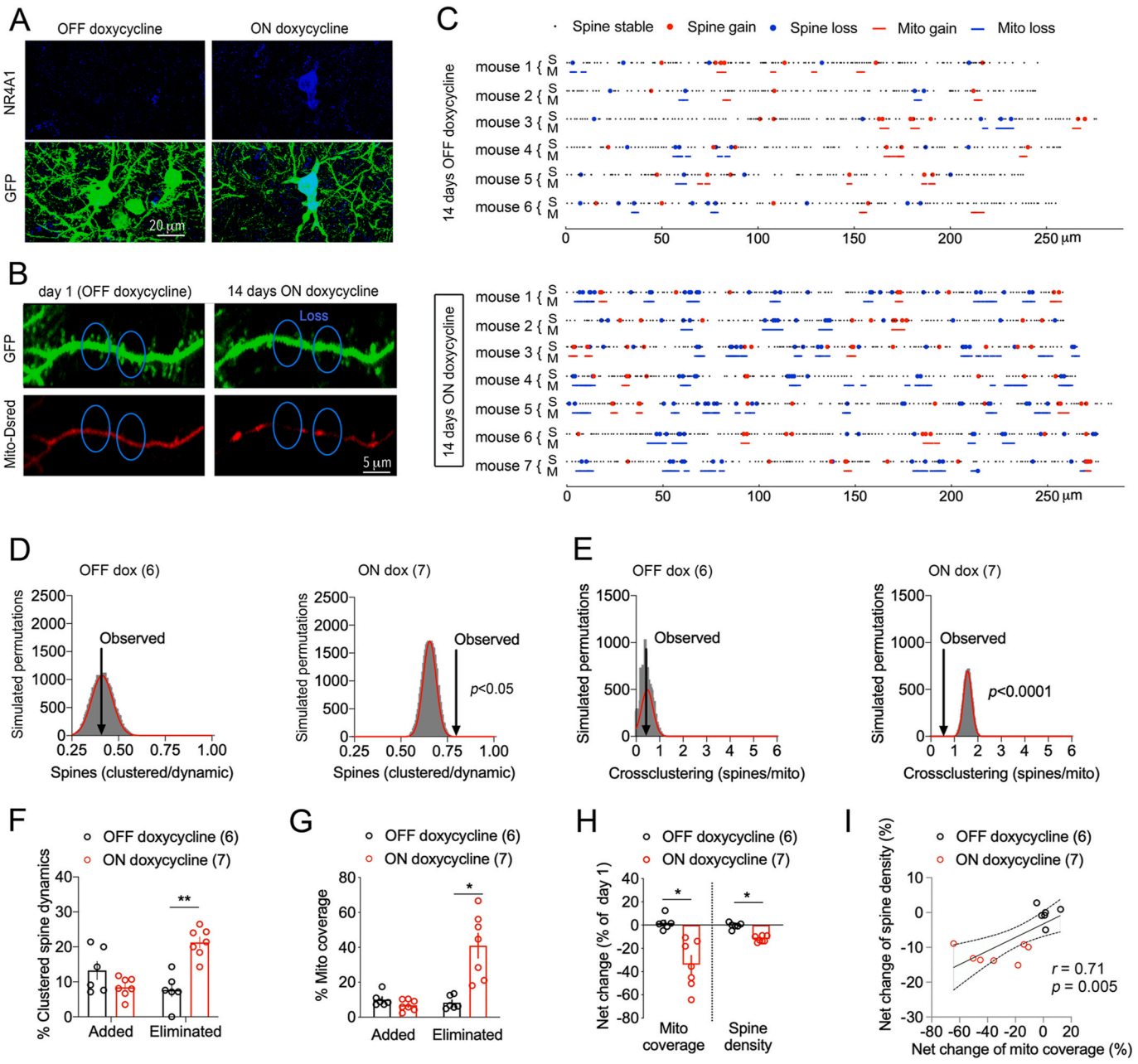

Fig. 7. Ectopic NR4A1 caused the loss of mitochondria and dendritic spine clusters.

A. Doxycycline-dependent expression of NR4A1 with a constitutive GFP reporter in layer 2/3 pyramidal neurons of somatosensory cortex (2 mg/ml dox in drinking water for 14 days).

B. Two-photon images of dendritic Mito-dsRed and GFP in pyramidal neurons electroporated with dox-dependent NR4A1. A distance ≤5 µm is indicated where the loss of dendritic spine clusters corresponded with the loss of mitochondrial coverage.

C. Topography of mitochondria and spine remodeling in dendritic territories imaged twice 14 days apart ± dox.

D. Clustered spine dynamics ON dox is greater than chance. Histogram shows the distribution of spine permutations in 30,000 simulations of randomized new spine positions (mean Gaussian fit = 0.41 ± 0.55, observed = 0.43 ± 0.12, N = 6 OFF, $p = 0.7$ and mean Gaussian fit = 0.65 ± 0.035, observed = 0.75 ± 0.11, N = 7 ON, $p = 0.04$).

E. Cross-clustering of spine dynamics and mito remodeling ON dox is greater than chance. Histogram shows the distribution of spine permutations in 30,000 simulations of randomized new spine positions with respect to mito remodeling (mean Gaussian fit = 0.46 ± 0.24, observed = 0.24 ± 0.11, N = 6 OFF, $p = 0.068$ and mean Gaussian fit = 1.56 ± 0.17, observed = 0.6 ± 0.12, N = 7 ON, $p < 0.0001$).

F. Gain/loss of clustered dendritic spines ≤5 µm. Two-way ANOVA: dox x clustered dynamics $F_{1,22} = 26.07$, $p < 0.0001$ post-hoc Tukey test: OFF vs ON groups $^{**}p < 0.0001$, N = 6 OFF, 7 ON mice.

G. Gain/loss of mitochondrial coverage. Two-way ANOVA: dox x mitochondria remodeling $F_{1,22} = 19.92$, $p = 0.0002$ post-hoc Tukey test: OFF vs ON groups $^{*}p < 0.0001$, N = 6 OFF, 7 ON mice.

H. Effect of dox on the net change of mitochondria coverage and spine density. Student two-tailed T-test comparing OFF and ON dox groups for mito $^{*}p = 0.02$ and spines $^{*}p = 0.002$, N = 6 OFF and 7 ON dox mice.

I. Pearson correlation between mitochondria and spine changes in dendritic territories of N = 6 OFF, 7 ON mice.

somatosensory cortex (Fig. S5). The ΔAF1 construct was electroporated with Mito-dsRed in cortex, and images acquired before and after chronic stress to track the effect on cross-clustering events (Fig. 8A and B). The observed data compared to the simulated spine permutations indicated that spine clustering and cross-clustering with proximal mitochondria are greater than chance ($p < 0.05$, Fig. 8C and D). The prolonged expression of ΔAF1 with dox treatment counteracted the effects of chronic stress on dendritic spine clustered dynamics (+261.7 ± 8.2% for additions and −53.7 ± 26.9% for eliminations, $p < 0.05$, Fig. 8E), on the total dynamics (+53 ± 14% for additions, $p = 0.03$ and −69.2 ± 3.1% for eliminations, $p < 0.0001$, Fig. S6B) as well as on mitochondrial remodeling (+146.5 ± 15% for additions and −77.9 ± 35% for eliminations, $p < 0.05$, Fig. 8F). Overall, ΔAF1 caused a net gain of spine number (+10 ± 3.2%, $p < 0.05$) and mitochondrial coverage (+9.7 ± 0.8%, $p < 0.05$, Fig. 8G) that correlated between animals and groups ($p < 0.05$, Fig. 8H). Results suggest that blocking NR4A1 during chronic stress prevented the clustered loss of dendritic spines and mitochondria.

4. Discussion

Here we showed that dendritic spine plasticity is intimately correlated with the remodeling of proximal mitochondrial network. Additions of newly formed spine clusters correlated with the extension of mitochondrial network; eliminations correlated with mitochondrial fragmentation. These observations made in dendrites of somatosensory cortex contrast with the lack of structural relationship between the dynamics of axon boutons and mitochondria in the visual cortex (Smit-Rigter et al., 2016). Other disparities that we observed between dendrites and axons in terms of mitochondrial motion are consistent with previous studies (Faits et al., 2016), suggesting that mitochondria behave quite differently between axons and dendrites, *in vitro* and *in vivo*, in juveniles and adults.

There are advantages to our study: (i) transcranial microscopy avoided unwanted inflammation that raises glucocorticoid levels; (ii) each subject serves as own control; (iii) fluorescent probes were prior validated *in vivo*; (iv) behavioral and chemical stimuli permitted measurements of adaptive and reactive mitochondrial responses; (v) pharmacogenetic approach avoided compensatory effects of constitutive expression; (vi) simulations excluded the possibility of random clustering events. There are also limitations: (i) observations in pyramidal neurons of somatosensory cortex may not be transposable to other types of neurons or brain regions; (ii) recordings were performed in anesthetized animals; (iii) excitation/emission spectra overlap between functional and structural probes precluded dual imaging; (iv) expression of probes declined with ageing precluding long term *in vivo* imaging; (v) RNA was analyzed from cortical extracts rather than purified pyramidal neurons due to difficulties with the extraction.

The topography of dendritic spine loss and mitochondria fragmentation highlighted hotspots of turnover, and that it takes more than a single dynamic spine within 5 μm to correlate with proximal mitochondria remodeling. Neighboring spines mostly responsive to distinct stimuli are usually coactive and likely involved in related experience circuit (Kleindienst et al., 2011). It is plausible that clustered spines are due to neighboring afferent axons from synchronized pre-synaptic neurons, which involved glutamate release (Takahashi et al., 2012). *In vitro* synapse-specific chemical-LTP induction and glutamate-uncaging also resulted in mitochondria fragmentation (Chen et al., 2018; Divakaruni et al., 2018), consistent with excess glutamate at cortical synapses on stress.

In the long-term, transcriptional regulation of mitochondrial fission/fusion and uncoupling genes could help rearrange the topography between spines and mitochondria as well as reduce the toxicity of high-rate oxidative phosphorylation in keeping with the buildup of chronic stress (Ježek et al., 2018). For example, 14 days of chronic stress increase the expression of fission genes *Fis1* and *Drp1* that likely contributes to the mechanism of mitochondrial fragmentation (Felix Kraus et al., 2021). These effects are further aggravated by an acute excitatory challenge after the 14 days of chronic stress with the downregulation of the fusion genes *Mfn1* and *Mfn2*. In this particular context, the downregulation of the fission genes *Opa1* and *Drp1* also indicate that the system is not collapsing but instead capable of adaptive plasticity to the new external and internal environments (Jeanneteau and Arango-Lievano, 2016). In stress-related pathologies such as Alzheimer's disease, high-resolution electron microscopy of post-mortem brains of animal models and patients revealed nanotubes between mitochondria as byproducts of mitochondrial fission arrest associated with altered brain energetics monitored with the PET ligand ^{18}F-fluorodeoxyglucose (Zhang et al., 2016). How the nanotubes interfere with the process of mitochondrial capture at the synapse is currently not understood (Jeanneteau and Arango-Lievano, 2016; Lee et al., 2018). A significant fraction of neuronal mitochondria constantly moves along microtubule networks in the axons while the remaining pool is captured where metabolic demand rises, notably at the pre-synapses and nodes of Ranvier (Chang et al., 2006; van Hameren et al., 2019). In the post-synapses, it is even more elusive given the difficultly to link morphologically a mitochondria with one particular dendritic spine given that mitochondria rarely penetrate through the neck of the spines (Kasthuri et al., 2015), and that it takes dynamics studies *in vivo* to reveal the physical cross-clustering between organelles.

The other example of transcriptional regulation is the switch of expression between the anion/proton transporters *Ucp2* and *Ucp4* that was also seen during cell fate transition between oxidative phosphorylation and aerobic glycolysis in conditions of chronic oxidative stress (Chu et al., 2009; Rupprecht et al., 2014). The mechanism of mitochondrial uncoupling is intended to reduce the toxicity associated with high-rates of oxidative phosphorylation without massive shortage in ATP stocks (Ježek et al., 2018). Why exchanging between UCPs is currently not understood. But the substrate specificity between UCP isoforms could represent a protective mechanism to limit the oxidative stress while retaining residual oxidative phosphorylation, a situation that we observed in the dendrites of pyramidal neurons after chronic stress. In principle, the ATP budget could be neutralized and oxidative damage limited if the management of the metabolic response to synaptic activity remained local and the balance of glycolysis to oxidative phosphorylation increased (Yellen, 2018). In times of intense energy demand, a shift of metabolism could serve the needs while maintaining neuronal safety. Neurons can elevate their own glycolysis in response to stimulation (Dıaz-Garcıa et al., 2017); yet they depend on dendritic mitochondria to fuel protein synthesis in specific synapses, indicating the crucial importance of local mitochondrial ATP synthesis (Rangaraju et al., 2019). The balance of glycolysis and oxidative phosphorylation in neurons is not understood and could vary between topography, states of rest and experience (Yellen, 2018) as do intracellular ATP levels between sleep-wake states (Natsubori et al., 2020). Neurons might temporarily use glycolysis over oxidative phosphorylation at specific synapses because it provides faster resupply of energy and lesser oxidative stress (Yellen, 2018).

When correlated, ATP and H2O2 productions predict enhanced oxidative phosphorylation. When ATP and H2O2 levels are not correlated in the same direction suggest a decoupling between energy production and redox signaling that is consistent with the regulation of UCP2/UCP4 expression after chronic stress. Measures of mitochondrial ATP and H2O2 levels reflect the net product of synthesis minus export or scavenging (van Hameren et al., 2019). $O2^{\cdot-}$ species are transformed by superoxide dismutase into H2O2 further processed by reducing enzymes into H2O and O2 (Ježek et al., 2018). So, it is possible that differences of ATP and H202 levels before and after stress could associate with the adaptive expression of the respiratory chain complexes, ADP/ATP translocase and antioxidant enzymes. The relative ATP and H2O2 levels reflect how the adjustments to chronic stress could prepare neurons to face future excitatory demand. For example, fragmented dendritic mitochondria responded to acute excitation with ATP and H2O2 levels

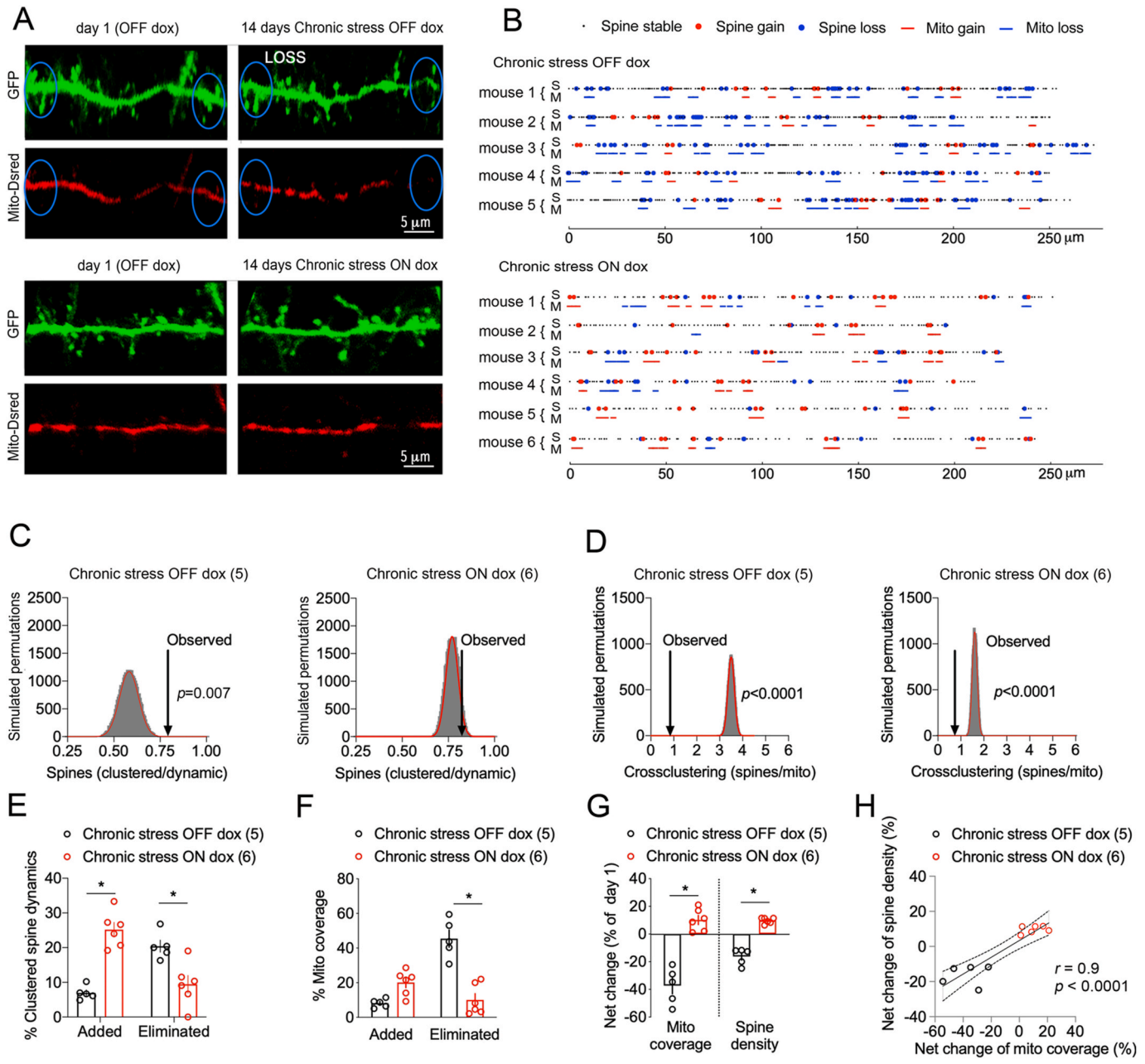

Fig. 8. Dominant-negative NR4A1 counteracted the effects of chronic stress.

A. Two-photon images of dendritic Mito-dsRed and GFP in pyramidal neurons electroporated with dox-dependent ΔAF1 in cortex of mice subjected to 14 days of stress.

B. Topography of mitochondria and spine remodeling in dendritic territories imaged twice 14 days apart ± dox.

C. Clustered spine dynamics on stress OFF dox is greater than chance. Histogram shows the distribution of spine permutations in 30,000 simulations of randomized new spine positions (mean Gaussian fit = 0.58 ± 0.51, observed = 0.76 ± 0.1, N = 5 OFF, $p = 0.007$ and mean Gaussian fit = 0.77 ± 0.03, observed = 0.84 ± 0.09, N = 6 ON, $p = 0.056$).

D. Cross-clustering of spine dynamics and mito remodeling on stress OFF dox is greater than chance. Histogram shows the distribution of spine permutations in 30,000 simulations of randomized new spine positions with respect to mito remodeling (mean Gaussian fit = 3.5 ± 0.14, observed = 0.85 ± 0.07, N = 5 OFF, $p <$ 0.0001 and mean Gaussian fit = 1.6 ± 0.1, observed = 0.71 ± 0.09, N = 6 ON, $p < 0.0001$).

E. Gain/loss of dendritic spines in clusters ≤5 µm. Two-way ANOVA: dox x clustered dynamics $F_{1,18} = 52.21$, $p < 0.0001$ post-hoc Tukey test: OFF vs ON dox groups *$p < 0.0001$, N = 5 OFF, 6 ON mice.

F. Gain/loss of mitochondrial dendritic coverage. Two-way ANOVA: dox x mitochondrial remodeling $F_{1,18} = 47.59$, $p < 0.0001$ post-hoc Tukey test: OFF vs ON dox groups *$p < 0.0001$, N = 5 OFF, 6 ON mice.

G. Effect of dox on the net change of mitochondrial coverage and spine density induced by chronic stress. Student two-tailed T-test comparing OFF and ON dox groups *$p < 0.0001$, N = 5 OFF and 6 ON dox mice.

H. Correlation (Pearson) between mitochondria and spine changes in dendritic territories of N = 5 OFF, 6 ON mice.

that correlated in the same direction, an indication of metabolic overdrive (Picard et al., 2014).

NR4A1 could program as a transcription factor the dynamic regulation of cellular metabolism in keeping with synaptic activity. For instance, NR4A1 signaling promotes cellular adaptation to different fuel utilization by modifying the expression of genes regulating mitochondrial oxidative phosphorylation, lipid oxidation and glycolysis (Zhang et al., 2020). If NR4A1 contributes to the programming of cell metabolism to its advantage in cancer, in the immune system (Liebmann et al., 2018; Thorne and Campbell, 2015), why couldn't it in neuronal cells? Dysregulated expression or activity of NR4A1 has been reported in the brain of animal models of stress, in the human brain of patients with major depressive disorders or with cognitive impairment associated with Alzheimer's disease (Jeanneteau et al., 2018). Although NR4A1 is still orphan of endogenous ligand, several synthetics molecules with agonistic or antagonistic effects have been put to good use for treating fibrosis, Parkinson's disease, autism spectrum disorders and diabetes (Kim et al., 2015; Li et al., 2016; Palumbo-Zerr et al., 2015; Safe et al., 2016; Spathis et al., 2017; Zhan et al., 2008). Targeting NR4A1 is a promising therapeutic strategy for combating maladaptation in these diseases.

5. Conclusion

One burden of cumulative stress is lesser energy production coupled with a loss of mitochondria and proximal dendritic spines that follows a probabilistic cross-clustering. More importantly, stressed mitochondria can increase energy production upon extraordinary excitation but at the expense of focal oxidation no longer buffered. Therefore, neurons prepare to face future excitatory demands by forming hotspots of plasticity for distributing the energetic burden of experience that builds up in keeping with synaptic activity. Future studies should focus on determining the causal relationship between the cross-clustering events and behavioral performance. We could not do this because *in utero* electroporation only targets sparse neurons unilaterally. Future application and development of mitochondria-targeted tools (Murphy and Hartley, 2018) will be instrumental to optimize mitochondrial functions during extreme challenges, physiological and pathological. For example, mitochondria-targeted optogenetic actuators (Rost et al., 2017; Tkatch et al., 2017) could help unearth how neurons manage the cost of living as foundation for the future bioenergetics studies in neurophysiology on one side, and in pathogenesis on the other side.

Funding

This study was funded by the Fondation pour la Recherche Médicale [Engineer-FRM 2016 and Equipe-FRM 2018].

CRediT authorship contribution statement

Yann Dromard: Formal analysis, Methodology. **Margarita Arango-Lievano:** Conceptualization, Formal analysis, Methodology. **Pierre Fontanaud:** Resources, Software. **Nicolas Tricaud:** Resources, Supervision, Writing. **Freddy Jeanneteau:** Conceptualization, Formal analysis, Funding acquisition, Methodology, Project administration, Resources, Supervision, Writing.

Declaration of competing interest

No authors are declaring a conflict of interest.

Data availability

Data posted on https://data.4tu.nl/account/articles/14737926

Acknowledgements

We thank J. Lu and Y. Zuo (UCSC, USA) for providing Matlab code.

Appendix A. Supplementary data

Supplementary data to this article can be found online at https://doi.org/10.1016/j.ynstr.2021.100402.

References

Albrecht, S., Barata, A., Grosshans, J., Teleman, A., Dick, T., 2011. In vivo mapping of hydrogen peroxide and oxidized glutathione reveals chemical and regional specificity of redox homeostasis. Cell Metabol. 14 (6), 819–829. https://doi.org/10.1016/j.cmet.2011.10.010.

Arango-Lievano, M., Borie, A.M., Dromard, Y., Murat, M., Desarmenien, M.G., Garabedian, M.J., Jeanneteau, F., 2019. Persistence of learning-induced synapses depends on neurotrophic priming of glucocorticoid receptors. Proc. Natl. Acad. Sci. U. S. A. 116 (26), 13097–13106. https://doi.org/10.1073/pnas.1903203116.

Arango-Lievano, M., Boussadia, B., De Terdonck, L.D.T., Gault, C., Fontanaud, P., Lafont, C., Mollard, P., Marchi, N., Jeanneteau, F., 2018. Topographic reorganization of cerebrovascular mural cells under seizure conditions. Cell Rep. 23 (4), 1045–1059. https://doi.org/10.1016/j.celrep.2018.03.110.

Arango-Lievano, M., Giannoni, P., Claeysen, S., Marchi, N., Jeanneteau, F., 2016a. Longitudinal in vivo imaging of the cerebrovasculature: relevance to CNS diseases. J Vis Exp 118, 54796. https://doi.org/10.3791/54796.

Arango-Lievano, M., Lambert, W.M., Bath, K.G., Garabedian, M.J., Chao, M.V., Jeanneteau, F., 2015. Neurotrophic-priming of glucocorticoid receptor signaling is essential for neuronal plasticity to stress and antidepressant treatment. Proc. Natl. Acad. Sci. U. S. A. 112 (51), 15737–15742. https://doi.org/10.1073/pnas.1509045112.

Arango-Lievano, M., Peguet, C., Catteau, M., Parmentier, M.L., Wu, S., Chao, M.V., Ginsberg, S.D., Jeanneteau, F., 2016b. Deletion of neurotrophin signaling through the glucocorticoid receptor pathway causes tau neuropathology. Sci. Rep. 6, 37231. https://doi.org/10.1038/srep37231.

Ashrafi, G., Wu, Z., Farrell, R., Ryan, T., 2017. GLUT4 mobilization supports energetic demands of active synapses. Neuron 93 (3). https://doi.org/10.1016/j.neuron.2016.12.020, 606-15e3.

Ayyasamy, V., Owens, K.M., Desouki, M.M., Liang, P., Bakin, A., Thangaraj, K., Buchsbaum, D.J., LoBuglio, A.F., Singh, K.K., 2011. Cellular model of Warburg effect identifies tumor promoting function of UCP2 in breast cancer and its suppression by genipin. PloS One 6 (9), e24792. https://doi.org/10.1371/journal.pone.0024792.

Bindokas, V.P., Lee, C.C., Colmers, W.F., Miller, R.J., 1998. Changes in mitochondrial function resulting from synaptic activity in the rat hippocampal slice. J. Neurosci. 18 (12), 4570–4587.

Chang, D.T., Honick, A.S., Reynolds, I.J., 2006. Mitochondrial trafficking to synapses in cultured primary cortical neurons. J. Neurosci. 26 (26), 7035–7045. https://doi.org/10.1523/JNEUROSCI.1012-06.2006.

Chavan, V., Willis, J., Walker, S.K., Clark, H.R., Liu, X., Fox, M.A., Srivastava, S., Mukherjee, K., 2015. Central presynaptic terminals are enriched in ATP but the majority lack mitochondria. PloS One 10 (4), e0125185. https://doi.org/10.1371/journal.pone.0125185.

Chen, C.C., Lu, J., Yang, R., Ding, J.B., Zuo, Y., 2018. Selective activation of parvalbumin interneurons prevents stress-induced synapse loss and perceptual defects. Mol Psychiatry 23 (7), 1614–1625. https://doi.org/10.1038/mp.2017.159.

Chen, Y., Wang, Y., Erturk, A., Kallop, D., Jiang, Z., Weimer, R.M., Kaminker, J., Sheng, M., 2014. Activity-induced Nr4a1 regulates spine density and distribution pattern of excitatory synapses in pyramidal neurons. Neuron. https://doi.org/10.1016/j.neuron.2014.05.027.

Chu, A., Ho, P., Kwok, K., Ho, J., Chan, K., Liu, H., Kung, M., Ramsden, D., Ho, S., 2009. Mitochondrial UCP4 attenuates MPP+- and dopamine-induced oxidative stress, mitochondrial depolarization, and ATP deficiency in neurons and is interlinked with UCP2 expression. Free radical biology & medicine 46 (6), 810–820. https://doi.org/10.1016/j.freeradbiomed.2008.12.015.

Delgado, T., Petralia, R., Freeman, D., Sedlacek, M., Wang, Y., Brenowitz, S., Sheu, S., Gu, J., Kapogiannis, D., Mattson, M., Yao, P., 2019. Comparing 3D ultrastructure of presynaptic and postsynaptic mitochondria. Biol Open 8 (8), bio044834. https://doi.org/10.1242/bio.044834.

Devine, M.J., Kittler, J.T., 2018. Mitochondria at the neuronal presynapse in health and disease. Nat. Rev. Neurosci. 19 (2), 63–80. https://doi.org/10.1038/nrn.2017.170.

Dıaz-Garcıa, C.M., Mongeon, R., Lahmann, C., Koveal, D., Zucker, H., Yellen, G., 2017. Neuronal stimulation triggers neuronal glycolysisand not lactate uptake. Cell Metabol. 26, 361–374. https://doi.org/10.1016/j.cmet.2017.06.021.

Divakaruni, S., Van Dyke, A., Chandra, R., LeGates, T., Contreras, M., Dharmasri, P., Higgs, H., Lobo, M., Thompson, S., Blanpied, T., 2018. Long-term potentiation requires a rapid burst of dendritic mitochondrial fission during induction. Neuron 100 (4), 860–875. https://doi.org/10.1016/j.neuron.2018.09.025 e7.

Erturk, A., Wang, Y., Sheng, M., 2014. Local pruning of dendrites and spines by caspase-3-dependent and proteasome-limited mechanisms. J. Neurosci. 34 (5), 1672–1688. https://doi.org/10.1523/JNEUROSCI.3121-13.2014.

Faits, M.C., Zhang, C., Soto, F., Kerschensteiner, D., 2016. Dendritic mitochondria reach stable positions during circuit development. eLife 5, e11583. https://doi.org/10.7554/eLife.11583.

Felix Kraus, F., Roy, K., Pucadyil, T.J., Ryan, M.T., 2021. Function and regulation of the divisome for mitochondrial fission. Nature 590 (7844), 57–66. https://doi.org/10.1038/s41586-021-03214-x.

Frank, A.C., Huang, S., Zhou, M., Gdalyahu, A., Kastellakis, G., Silva, T.K., Lu, E., Wen, X., Poirazi, P., Trachtenberg, J.T., Silva, A.J., 2018. Hotspots of dendritic spine turnover facilitate clustered spine addition and learning and memory. Nat. Commun. 9 (1), 422. https://doi.org/10.1038/s41467-017-02751-2.

Fu, M., Yu, X., Lu, J., Zuo, Y., 2012. Repetitive motor learning induces coordinated formation of clustered dendritic spines in vivo. Nature 483 (7387), 92–95. https://doi.org/10.1038/nature10844.

Fu, Z., Tan, X., Fang, H., Lau, P., Wang, X., Cheng, H., Bi, G., 2017. Dendritic mitoflash as a putative signal for stabilizing long-term synaptic plasticity. Nat. Commun. 8 (1), 31. https://doi.org/10.1038/s41467-017-00043-3.

Harris, J.J., Jolivet, R., Attwell, D., 2012. Synaptic energy use and supply. Neuron 75 (5), 762–777. https://doi.org/10.1016/j.neuron.2012.08.019.

Jang, S., Nelson, J.C., Bend, E.G., Rodríguez-Laureano, L., Tueros, F.G., Cartagenova, L., Underwood, K., Jorgensen, E.M., Colón-Ramos, D.A., 2016. Glycolytic enzymes localize to synapses under energy stress to support synaptic function. Neuron 90 (2), 278–291. https://doi.org/10.1016/j.neuron.2016.03.011.

Jeanneteau, F., Arango-Lievano, M., 2016. Linking mitochondria to synapses: new insights for stress-related neuropsychiatric disorders. Neural Plast. 2016, 3985063. https://doi.org/10.1155/2016/3985063.

Jeanneteau, F., Barrere, C., Vos, M., De Vries, C.J., Rouillard, C., Levesque, D., Dromard, Y., Moisan, M.P., Duric, V., Franklin, T.C., Duman, R.S., Lewis, D.A., Ginsberg, S.D., Arango-Lievano, M., 2018. The stress-induced transcription factor NR4A1 adjusts mitochondrial function and synapse number in prefrontal cortex. J. Neurosci. 38 (6), 1335–1350. https://doi.org/10.1523/JNEUROSCI.2793-17.2017.

Jeanneteau, F., Deinhardt, K., Miyoshi, G., Bennett, A.M., Chao, M.V., 2010. The MAP kinase phosphatase MKP-1 regulates BDNF-induced axon branching. Nat. Neurosci. 13 (11), 1373–1379 nn.2655 [pii], 10.1038/nn.2655.

Ježek, P., Holendová, B., Garlid, K., M, J., 2018. Mitochondrial uncoupling proteins. Subtle Regulators of Cellular Redox Signaling Antioxidants & redox signaling 29 (7), 667–714. https://doi.org/10.1089/ars.2017.7225.

Kasthuri, N., Hayworth, K.J., Berger, D.R., Schalek, R.L., Conchello, J.A., Knowles-Barley, S., Lee, D., Vazquez-Reina, A., Kaynig, V., Jones, T.R., Roberts, M., Morgan, J.L., Tapia, J.C., Seung, H.S., Roncal, W.G., Vogelstein, J.T., Burns, R., Sussman, D.L., Priebe, C.E., Pfister, H., Lichtman, J.W., 2015. Saturated reconstruction of a volume of neocortex. Cell 162 (3), 648–661. https://doi.org/10.1016/j.cell.2015.06.054.

Kim, C.H., Han, B.S., Moon, J., Kim, D.J., Shin, J., Rajan, S., Nguyen, Q.T., Sohn, M., Kim, W.G., Han, M., Jeong, I., Kim, K.S., Lee, E.H., Tu, Y., Naffin-Olivos, J.L., Park, C.H., Ringe, D., Yoon, H.S., Petsko, G.A., Kim, K.S., 2015. Nuclear receptor Nurr1 agonists enhance its dual functions and improve behavioral deficits in an animal model of Parkinson's disease. Proc. Natl. Acad. Sci. U. S. A. 112 (28), 8756–8761. https://doi.org/10.1073/pnas.1509742112.

Kirov, S., Fomitcheva, I., Sword, J., 2020. Rapid neuronal ultrastructure disruption and recovery during spreading depolarization-induced cytotoxic edema. Cereb Cortex 30 (10), 5517–5531. https://doi.org/10.1093/cercor/bhaa134.

Kislin, M., Sword, J., Fomitcheva, I., Croom, D., Pryazhnikov, E., Lihavainen, E., Toptunov, D., Rauvala, H., Ribeiro, A., Khiroug, L., Kirov, S., 2017. Reversible disruption of neuronal mitochondria by ischemic and traumatic injury revealed by quantitative two-photon imaging in the neocortex of anesthetized mice. J. Neurosci. 37 (2), 333–348. https://doi.org/10.1523/JNEUROSCI.1510-16.2016.

Kleindienst, T., Winnubst, J., Roth-Alpermann, C., Bonhoeffer, T., Lohmann, C., 2011. Activity-dependent clustering of functional synaptic inputs on developing hippocampal dendrites. Neuron 72 (6), 1012–1024. https://doi.org/10.1016/j.neuron.2011.10.015.

Kwon, S., Sando, R.r., Lewis, T., Hirabayashi, Y., Maximov, A., Polleux, F., 2016. LKB1 regulates mitochondria-dependent presynaptic calcium clearance and neurotransmitter release properties at excitatory synapses along cortical axons. PLoS Biol. 47 (7), e1002516 https://doi.org/10.1371/journal.pbio.1002516.

Lee, A., Hirabayashi, Y., Kwon, S., Lewis, T.J., Polleux, F., 2018. Emerging roles of mitochondria in synaptic transmission and neurodegeneration. Curr Opin Physiol 3, 82–93. https://doi.org/10.1016/j.cophys.2018.03.009.

Li, H., Zhao, P., Xu, Q., Shan, S., Hu, C., Qiu, Z., Xu, X., 2016. The autism-related gene SNRPN regulates cortical and spine development via controlling nuclear receptor Nr4a1. Sci. Rep. 6, 29878. https://doi.org/10.1038/srep29878.

Li, Z., Okamoto, K., Hayashi, Y., Sheng, M., 2004. The importance of dendritic mitochondria in the morphogenesis and plasticity of spines and synapses. Cell 119 (6), 873–887. https://doi.org/10.1016/j.cell.2004.11.003.

Liebmann, M., Hucke, S., Koch, K., Eschborn, M., Ghelman, J., Chasan, A.I., Glander, S., Schädlich, M., Kuhlencord, M., Daber, N.M., Eveslage, M., Beyer, M., Dietrich, M., Albrecht, P., Stoll, M., Busch, K.B., Wiendl, H., Roth, J., Kuhlmann, T., Klotz, L., 2018. Nur77 serves as a molecular brake of the metabolic switch during T cell activation to restrict autoimmunity. Proc. Natl. Acad. Sci. U. S. A. 115 (34), E8017–E8026. https://doi.org/10.1073/pnas.1721049115.

Lin, M., Beal, M., 2006. Mitochondrial dysfunction and oxidative stress in neurodegenerative diseases. Nature 443 (7113), 787–795. https://doi.org/10.1038/nature05292.

Lin, Y., Li, L., Nie, W., Liu, X., Adler, A., Xiao, C., Lu, F., Wang, L., Han, H., Wang, X., Gan, W.B., Cheng, H., 2019. Brain activity regulates loose coupling between mitochondrial and cytosolic Ca2+ transients. Nature communication 10 (1), 5277. https://doi.org/10.1038/s41467-019-13142-0.

Liu, D., Chan, S., de Souza-Pinto, N., Slevin, J., Wersto, R., Zhan, M., Mustafa, K., de Cabo, R., Mattson, M., 2006. Mitochondrial UCP4 mediates an adaptive shift in energy metabolism and increases the resistance of neurons to metabolic and oxidative stress. NeuroMolecular Med. 8 (3), 389–414. https://doi.org/10.1385/NMM:8:3:389.

Mattson, M.P., Gleichmann, M., Cheng, A., 2008. Mitochondria in neuroplasticity and neurological disorders. Neuron 60 (5), 748–766. https://doi.org/10.1016/j.neuron.2008.10.010.

Murphy, M.P., Hartley, R.C., 2018. Mitochondria as a therapeutic target for common pathologies. Nat. Rev. Drug Discov. 17 (12), 865–886. https://doi.org/10.1038/nrd.2018.174.

Natsubori, A., Tsunematsu, T., Karashima, A., Imamura, H., Kabe, N., Trevisiol, A., Hirrlinger, J., Kodama, T., Sanagi, T., Masamoto, K., Takata, N., Nave, K., Matsui, K., Tanaka, K., Honda, M., 2020. Intracellular ATP levels in mouse cortical excitatory neurons varies with sleep–wake states. Commnunications Biology 3 (1), 491. https://doi.org/10.1038/s42003-020-01215-6.

Palumbo-Zerr, K., Zerr, P., Distler, A., Fliehr, J., Mancuso, R., Huang, J., Mielenz, D., Tomcik, M., Furnrohr, B.G., Scholtysek, C., Dees, C., Beyer, C., Kronke, G., Metzger, D., Distler, O., Schett, G., Distler, J.H., 2015. Orphan nuclear receptor NR4A1 regulates transforming growth factor-beta signaling and fibrosis. Nat. Med. 21 (2), 150–158. https://doi.org/10.1038/nm.3777.

Pathak, D., Shields, L.Y., Mendelsohn, B.A., Haddad, D., Lin, W., Gerencser, A.A., Kim, H., Brand, M.D., Edwards, R.H., Nakamura, K., 2015. The role of mitochondrially derived ATP in synaptic vesicle recycling. J. Biol. Chem. 290 (37), 22325–22336. https://doi.org/10.1074/jbc.M115.656405.

Picard, M., Juster, R.P., McEwen, B.S., 2014. Mitochondrial allostatic load puts the 'gluc' back in glucocorticoids. Nat. Rev. Endocrinol. 10 (5), 303–310. https://doi.org/10.1038/nrendo.2014.22.

Picard, M., McEwen, B., Epel, E., Sandi, C., 2018. An energetic view of stress: focus on mitochondria. Front. Neuroendocrinol. 49, 72–85. https://doi.org/10.1016/j.yfrne.2018.01.001.

Rangaraju, V., Lauterbach, M., Schuman, E., 2019. Spatially stable mitochondrial CompartmentsFuel local translation during plasticity. Cell 176, 73–84. https://doi.org/10.1016/j.cell.2018.12.013.

Rost, B.R., Schneider-Warme, F., Schmitz, D., Hegemann, P., 2017. Optogenetic tools for subcellular applications in neuroscience. Neuron 96 (3), 572–603. https://doi.org/10.1016/j.neuron.2017.09.047.

Rowley, S., Patel, M., 2013. Mitochondrial involvement and oxidative stress in temporal lobe epilepsy Free. Radic Biol Med 62, 121–131. https://doi.org/10.1016/j.freeradbiomed.2013.02.002.

Rupprecht, A., Sittner, D., Smorodchenko, A., Hilse, K., Goyn, J., Moldzio, R., Seiler, A., Bräuer, A., Pohl, E., 2014. Uncoupling protein 2 and 4 expression pattern during stem cell differentiation provides new insight into their putative function. PloS One 9 (2), e88474. https://doi.org/10.1371/journal.pone.0088474.eCollection2014.

Safe, S., Jin, U.H., Morpurgo, B., Abudayyeh, A., Singh, M., Tjalkens, R.B., 2016. Nuclear receptor 4A (NR4A) family - orphans no more. J. Steroid Biochem. Mol. Biol. 157, 48–60. https://doi.org/10.1016/j.jsbmb.2015.04.016.

Smit-Rigter, L., Rajendran, R., Silva, C., Spierenburg, L., Groeneweg, F., Ruimschotel, E., van Versendaal, D., van der Togt, C., Eysel, U., Heimel, J., Lohmann, C., Levelt, C., 2016. Mitochondrial dynamics in visual cortex are limited in vivo and not affected by axonal structural plasticity. Curr. Biol. 26 (19), 2609–2616. https://doi.org/10.1016/j.cub.2016.07.033.

Sobieski, C., Fitzpatrick, M., Mennerick, S., 2017. Differential presynaptic ATP supply for basal and high-demand transmission. J. Neurosci. 37 (7), 1888–1899. https://doi.org/10.1523/JNEUROSCI.2712-16.2017.

Spathis, A.D., Asvos, X., Ziavra, D., Karampelas, T., Topouzis, S., Cournia, Z., Qing, X., Alexakos, P., Smits, L.M., Dalla, C., Rideout, H.J., Schwamborn, J.C., Tamvakopoulos, C., Fokas, D., Vassilatis, D.K., 2017. Nurr1:RXRα heterodimer activation as monotherapy for Parkinson's disease. Proc. Natl. Acad. Sci. U. S. A. 114 (15), 3999–4004. https://doi.org/10.1073/pnas.1616874114.

Takahashi, N., Kitamura, K., Matsuo, N., Mayford, M., Kano, M., Matsuki, N., Ikegaya, Y., 2012. Locally synchronized synaptic inputs. Science 335 (6066), 353–356. https://doi.org/10.1126/science.1210362.

Terada, T., Obi, T., Bunai, T., Matsudaira, T., Yoshikawa, E., Ando, I., Futatsubashi, M., Tsukada, H., Ouchi, Y., 2020. In vivo mitochondrial and glycolytic impairments in patients with Alzheimer disease. Neurology 94 (5), e1592–e1604. https://doi.org/10.1212/WNL.0000000000009249.

Thorne, J.L., Campbell, M.J., 2015. Nuclear receptors and the Warburg effect in cancer. Int J Cancer 137 (7), 1519–1527. https://doi.org/10.1002/ijc.29012.

Tkatch, T., Greotti, E., Baranauskas, G., Pendin, D., Roy, S., Nita, L.I., Wettmarshausen, J., Prigge, M., Yizhar, O., Shirihai, O.S., Fishman, D., Hershfinkel, M., Fleidervish, I.A., Perocchi, F., Pozzan, T., Sekler, I., 2017. Optogenetic control of mitochondrial metabolism and Ca2+ signaling by mitochondria-targeted opsins. Proc. Natl. Acad. Sci. U. S. A. 114 (26), E5167–E5176. https://doi.org/10.1073/pnas.1703623114.

Vaccaro, V., Devine, M., Higgs, N., Kittler, J., 2017. Miro1-dependent mitochondrial positioning drives the rescaling of presynaptic Ca2+ signals during homeostatic plasticity. EMBO Rep. 18 (2), 231–240. https://doi.org/10.15252/embr.201642710.

van Hameren, G., Campbell, G., Deck, M., Berthelot, J., Gautier, B., Quintana, P., Chrast, R., Tricaud, N., 2019. In vivo real-time dynamics of ATP and ROS production in axonal mitochondria show decoupling in mouse models of peripheral neuropathies. Acta Neuropathol Commun 7 (7), 86. https://doi.org/10.1186/s40478-019-0740-4.

Virlogeux, A., Moutaux, E., Christaller, W., Genoux, A., Bruyère, J., Fino, E., Charlot, B., Cazorla, M., Saudou, F., 2018. Reconstituting corticostriatal network on-a-Chip reveals the contribution of the presynaptic compartment to huntington's disease. Cell Rep. 22 (1), 110–122. https://doi.org/10.1016/j.celrep.2017.12.013.

Yellen, G., 2018. Fueling thought: management of glycolysis and oxidative phosphorylation in neuronal metabolism. J. Cell Biol. 217 (7), 2235–2246. https://doi.org/10.1083/jcb.201803152.

Yohn, N.L., Blendy, J.A., 2017. Adolescent chronic unpredictable stress exposure is a sensitive window for long-term changes in adult behavior in mice. Neuropsychopharmacology 42 (8), 1670–1678. https://doi.org/10.1038/npp.2017.11.

Yoshida, T., Alfaqaan, S., Sasaoka, N., Imamura, H., 2017. Application of FRET-based biosensor "ATeam" for visualization of ATP levels in the mitochondrial matrix of living mammalian cells methods. Mol Biol 1567, 231–243. https://doi.org/10.1007/978-1-4939-6824-4_14.

Zhan, Y., Du, X., Chen, H., Liu, J., Zhao, B., Huang, D., Li, G., Xu, Q., Zhang, M., Weimer, B.C., Chen, D., Cheng, Z., Zhang, L., Li, Q., Li, S., Zheng, Z., Song, S., Huang, Y., Ye, Z., Su, W., Lin, S.C., Shen, Y., Wu, Q., 2008. Cytosporone B is an agonist for nuclear orphan receptor Nur77. Nat. Chem. Biol. 4 (9), 548–556 nchembio.106 [pii], 10.1038/nchembio.106.

Zhang, C., Zhang, B., Zhang, X., Sun, G., Sun, X., 2020. Targeting orphan nuclear receptors NR4As for energy homeostasis and diabetes. Front. Pharmacol. 11, 587457. https://doi.org/10.3389/fphar.2020.587457.

Zhang, L., Trushin, S., Christensen, T.A., Bachmeier, B.V., Gateno, B., Schroeder, A., Yao, J., Itoh, K., Sesaki, H., Poon, W.W., Gylys, K.H., Patterson, E.R., Parisi, J.E., Diaz Brinton, R., Salisbury, J.L., Trushina, E., 2016. Altered brain energetics induces mitochondrial fission arrest in Alzheimer's Disease. Sci. Rep. 6, 18725. https://doi.org/10.1038/srep18725.

Zhang, S.J., Zou, M., Lu, L., Lau, D., Ditzel, D.A., Delucinge-Vivier, C., Aso, Y., Descombes, P., Bading, H., 2009. Nuclear calcium signaling controls expression of a large gene pool: identification of a gene program for acquired neuroprotection induced by synaptic activity. PLoS Genet. 5 (8), e1000604 https://doi.org/10.1371/journal.pgen.1000604.